RELATION BETWEEN THE LUMINOSITY OF YOUNG STELLAR OBJECTS AND THEIR CIRCUMSTELLAR ENVIRONMENT

Dejan Vinković

Institute for Advanced Study, School of Natural Sciences, Princeton, NJ; dejan@ias.edu

AND

Tomislav Jurkić

Physics Department, University of Rijeka, Rijeka, Croatia

Received 2006 August 20; accepted 2006 November 29

ABSTRACT

We present a new model-independent method of comparison of NIR visibility data of YSOs. The method is based on scaling the measured baseline with the YSO's distance and luminosity, which removes the dependence of visibility on these two variables. We use this method to compare all available NIR visibility data and demonstrate that it distinguishes YSOs of luminosity $L_\star \lesssim 10^3 \ L_\odot$ (low L) from YSOs of $L_\star \gtrsim 10^3 \ L_\odot$ (high L). This confirms earlier suggestions, based on fits of image models to the visibility data, for the difference between the NIR sizes of these two luminosity groups. When plotted against the "scaled" baseline, the visibility creates the following data clusters: low-L Herbig Ae/Be stars, T Tauri stars, and high-L Herbig Be stars. We model the shape and size of clusters with different image models and find that low-L Herbig stars are best explained by the uniform brightness ring and the halo model, T Tauri stars with the halo model, and high-L Herbig stars with the accretion disk model. However, the plausibility of each model is not well established. Therefore, we try to build a descriptive model of the circumstellar environment consistent with various observed properties of YSOs. We argue that low-L YSOs have optically thick disks with the optically thin inner dust sublimation cavity and an optically thin dusty outflow above the inner disk regions. High-L YSOs have optically thick accretion disks with high accretion rates enabling gas to dominate the NIR emission over dust. Although observations would favor such a description of YSOs, the required dust distribution is not supported by our current understanding of dust dynamics.

Subject headings: accretion, accretion disks — circumstellar matter — instrumentation: interferometers — radiative transfer — stars: formation — stars: pre–main-sequence

1. INTRODUCTION

Young stellar objects (YSOs) are surrounded by dust and gas leftovers from the process of star formation. Observations have revealed that this material concentrates into a (protoplanetary) disk accreting toward the central star. The disk undergoes the process of dust and gas coagulation and formation of larger objects, eventually resulting in a planetary system. Hence, YSOs are of a topical astronomical interest because they can help us understand how planetary systems form and evolve.

Dust in the disk is very efficient in absorbing the stellar radiation. It makes the disk appear optically thick until the dust is either removed or coagulated into larger objects. Dust is also a very efficient tracer of protoplanetary disks in infrared, where dust reemits the energy that it absorbed from the star. Direct imaging has proved to be especially useful in unraveling properties of YSOs. Depending on the wavelength, images capture different temperature zones and optical depths of the protoplanetary dusty disk. From the terrestrial planet formation perspective, the most interesting is the inner few AU of the disk. In this zone dust temperatures can reach a thousand degrees or more. At these temperatures dust either sublimates or becomes heavily thermally processed, and it emits in the near-infrared (NIR). Unfortunately, the angular size of this zone is on the milliarcsecond scale and until recently unresolvable.

Thanks to advances in NIR interferometry (e.g., Monnier 2003), the inner regions of many YSO disks have been resolved to date. One of the first surprises coming out of these observations is a significantly larger NIR size than previously predicted from theoretical models of accretion disks (Monnier & Millan-Gabet 2002; Tuthill et al. 2001). This led to revisions of the existing theories of disk

structure by invoking an optically thin inner disk hole around the star. The hole is clear of dust because of its sublimation, while the gas is unable to provide a considerable optical thickness. On the other hand, the spectrum shows that the inner disk emits much more NIR flux than expected from a simple flat disk. This directly implies that the disk structure has to flare up in the zone where it reaches its dust sublimation temperature ($T_s \sim 1500-2000$ K) in order to increase its NIR-emitting area. Such a model was described by Dullemond et al. (2001), where the disk is vertically puffed up at the inner disk rim because of the direct stellar heating of the disk interior.

Unfortunately, the NIR interferometric observations were capable of providing only the characteristic size of the emitting region, but they were not good enough to constrain the exact geometry of this region. It is only the most recent observations that manage to make a step further and detect deviations from simple centrally symmetric images (Monnier et al. 2006). These deviations turned out to be surprisingly small, unlike strong brightness asymmetries predicted by inclined disk models of Dullemond et al. (2001). Such a result favors a derivative of this model where the inner disk rim does not create a vertically flat wall, but rather a curved surface (Isella & Natta 2005). In addition, it is still not clear from the data if an additional dusty wind component coexists with the disk and contributes to the images and NIR flux. According to Vinković et al. (2006), such an optically thin halo around the inner disk can completely explain the NIR flux without a need for the disk puffing.

Another major result coming out of the NIR interferometric data is the dependence of inner disk size on luminosity (Monnier & Millan-Gabet 2002; Monnier et al. 2005). The size was derived by fitting ad hoc uniform brightness ring image models to the

measured visibilities. The inner ring radius $R_{\rm in}$, which is assumed to be the dust sublimation radius of the disk, is plotted against the luminosity $L_\star$ of the observed object. The expected trend $R_{\rm in} \propto L_\star^{1/2}$ is followed by YSOs of $L_\star < 10^3 \, L_\odot$, with sublimation temperatures between 1000 and 1500 K. Objects with $L_\star > 10^3 \, L_\odot$ deviate from this trend by having considerably smaller inner radius than expected. Monnier et al. (2005) argue that high-luminosity objects have optically thick gas within the inner dust-free disk hole. This would shield the dust from direct stellar heating and enable the dust to survive closer to the star, resulting in a smaller inner ring radius.

The basic approach in these studies is to use predefined theoretical models and correlate the object's luminosity with a model parameter derived from fitting the model to the visibility data. This inevitably leads to questions on the validity of the model and conclusions derived from it. This is especially true for models of inner disks, considering the large uncertainties about the inner disk geometry and dust properties. In this paper we propose an approach that can detect visibility dependence on luminosity without invoking any model of dust geometry. The approach is based on scaling the baseline value such that all objects seemingly appear located at the same distance from us and have the same luminosity.

We collected all available NIR visibility data on YSOs (13 T Tau, 27 Herbig Ae/Be, and 4 FU Ori stars) in the literature, and in § 2 we compare their scaled visibilities. We confirm that the circumstellar environment of objects with $L_\star > 10^3 \, L_\odot$ differs from less luminous objects, with high-L objects showing smaller structures. In § 3 we plot scaled theoretical visibilities of a uniform brightness ring, dusty halo, and accretion disk over the scaled measured visibilities and explore the range of model parameters that are needed for accommodating all the data. In § 4 we present an extensive discussion of various observational aspects of YSOs, with special attention given to the differences between low- and high-L YSOs. We try to sketch a self-consistent model that would explain various observed properties of YSOs. The summary of the paper is given in § 5.

2. YSO VISIBILITIES WITH SCALED BASELINES

Studies of the relation between YSO luminosities and their NIR visibilities have been based on fitting the constant surface brightness ring image model to the visibility data. The obtained inner ring radius is then correlated with the luminosity, where the basic assumption is that this radius is equivalent to the dust sublimation distance from the star (Monnier & Millan-Gabet 2002; Eisner et al. 2004; Monnier et al. 2005; Akeson et al. 2005b). A slightly different approach is used by Vinković et al. (2006), who use a dusty halo model, but the approach is still based on obtaining the sublimation radius from the fit to visibility data. Using this approach, Eisner et al. (2004) and Monnier et al. (2005) showed that YSOs with luminosity $\gtrsim 10^3 \, L_\odot$ have a significantly smaller inner ring radius than less luminous objects.

It is, however, not clear if the ring model is a plausible model for fitting the visibility. The NIR disk surface brightness is not a uniform ring, but a complicated function that critically depends on dust emission and scattering properties and the disk optical depth structure. Moreover, Vinković et al. (2006) used a halo model and obtained a significantly smaller scatter of inner halo radius with luminosity. Here we show that, when exploring correlations between luminosity and visibility data, all uncertainties due to different models of circumstellar dust properties and geometry can be avoided by model-independent scaling of visibility.

The visibility $V(B)$ is a function of the spatial frequency B, also called baseline. It consists of two individual additive visibilities:

stellar and diffuse. The stellar contribution to the NIR visibility at currently used baselines is a constant because the star remains unresolved. The NIR diffuse part is a contribution from the circumstellar dust emission and scattering, while the gas brightness can be neglected (we see later on that this is not true for luminous YSOs).

The diffuse visibility critically depends on two parameters: (1) distance to the object, which affects the angular size of the image on the sky, and (2) physical size of the object, which is controlled by dust radiative transfer. The equations of dust radiative transfer have powerful intrinsic scaling properties according to which luminosity and linear dimensions are irrelevant for solving the equations (Ivezić & Elitzur 1997). Overall luminosity is never an input parameter: only the source spectral shape is important. Also, absolute scales of dust densities and distances are irrelevant: only the optical depth, geometrical angles, relative thicknesses, and aspect ratios enter the equations. Luminosity is important only when we need to translate dimensionless radiative transfer solutions to physical units, where physical dimensions scale with $L_\star^{1/2}$ (eq. [27] in Ivezić & Elitzur 1997).

When comparing intrinsic properties of the circumstellar dust geometry of two objects in the sky, we want to make sure that detected size differences are not due to (1) differences in distances and (2) size scaling due to different luminosities. Therefore, we first need to scale objects to the same luminosity and to the same distance. Visibility of an image is inversely proportional to the characteristic angular size of the image (Ivezić & Elitzur 1996). In turn, the angular size is inversely proportional to distance D but, as we argue from the radiative transfer scaling properties, proportional to $L_\star^{1/2}$. Hence, we define the *scaled baseline*

$$B_{\rm scaled} = B \frac{\sqrt{L_\star/L_\odot}}{D/{\rm pc}}, \qquad (1)$$

which has the same physical units as the ordinary baseline, but it removes the intrinsic dependence on distance and radiative transfer scaling.

Although this scaling can be postulated for any system, it is meaningful only for systems with a central heating source. Binary systems, for example, can have entirely different scaling properties. Notice, however, that the method is useful for disks with significant accretion luminosities because most of the accretion luminosity comes from the accretion shock. Hence, the dust in such disks is exposed primarily to the sum of stellar and accretion luminosity $L_\star + L_{\rm acc}$, and this sum should replace the luminosity factor in equation (1).

We collected all objects with available H- and K-band visibility data and list them in Table 1: 13 objects classified as T Tauri stars, 27 Herbig Ae/Be stars, and 4 FU Orionis objects. We excluded from the list objects that are most probably B[e] supergiants (MWC 349A, MWC 342, HD 45677, HD 58647) and show them separately only for illustration. Since the goal is to compare overall trends in visibility, we average the visibility data within bins of about 0.5 Mλ in objects that have many measurements taken at similar baselines (the lower and upper visibility limits are shown in the table when applicable). For a more detailed view of the visibility data in individual objects, we suggest following the references given in the table.

Figures 1 and 2 show the visibility data when plotted against the scaled baseline. The difference between low-luminosity ($L_\star \lesssim 10^3 \, L_\odot$, low L) and high-luminosity ($L_\star \gtrsim 10^3 \, L_\odot$, high L) Herbig Ae/Be objects is now clearly visible. It is important to emphasize that this is a *model-independent* detection of intrinsic differences

TABLE 1
OBJECT PROPERTIES AND AVERAGED VISIBILITY DATA

| | | | | | | VISIBILITY AVERAGES | | |
OBJECT NAMES	DISTANCE (pc)	DISTANCE REF.	LUMINOSITY ($L_\odot$)	LUMINOSITY REF.	Baseline (Mλ)	H Band	K Band	Visibility Ref.
				T Tau Objects				
LkCa 15	142±14	1	0.74	2	35.5	...	0.95	2
BP Tau	142±14	1	0.83	2	37.5	...	0.93	2
DR Tau	142±14	1	1.28±0.50	3	38.0	...	0.84–1.03	4
	142±14	1	1.28±0.50	3	48.9	...	0.87–0.95	
GM Aur................................	142±14	1	1.01	2	33.3	...	0.93	2
AS 205A	165±20	5	7.8±6.5	6	25.0	...	0.66–0.97	6
	165±20	5	7.8±6.5	6	37.0	...	0.79–0.85	
HD 143006	94±35	7	1.4±0.5	7	25.5	...	0.93	7
	94±35	7	1.4±0.5	7	26.9	...	0.97	
RW Aur	142±14	1	1.7	2	39.0	...	0.78	2
AS 207A	165±20	5	2.9±0.2	6	25.5	...	0.79–0.96	6
V2508 Oph	165±20	5	4.1±0.8	6	27.0	...	0.77–1.00	6
DG Tau	142±14	1	3.62	2	38.8	...	0.57–0.65	2, 8
T Tau N..............................	142±14	1	7.3	9	38.5	...	0.48–0.77	4, 10, 11
	142±14	1	7.3	9	48.5	...	0.32–0.80	
RY Tau	142±14	1	10±7	3, 12	6.0	0.85–0.95	...	4, 12
	142±14	1	10±7	3, 12	17.5	0.75–0.82	...	
	142±14	1	10±7	3, 12	38.5	...	0.52–0.70	
	142±14	1	10±7	3, 12	49.5	...	0.16–0.55	
SU Aur	142±14	1	13.5±0.7	3	38.0	...	0.64–1.04	4, 10, 11
	142±14	1	13.5±0.7	3	49.5	...	0.55–0.95	
				Herbig Ae/Be Objects				
PX Vul	420	13	26.2±12.5	6	38.5	...	0.75–0.92	6
CQ Tau................................	104±21	14	4.2±3.8	14, 15	38.0	...	0.55–0.67	16
	104±21	14	4.2±3.8	14, 15	48.5	...	0.59–0.67	
HD 142666	116	17	8.8±2.5	7	34.1	...	0.78	7
	116	17	8.8±2.5	7	36.3	...	0.67–0.77	
	116	17	8.8±2.5	7	37.5	...	0.75	
HD 144432	145	18	14.5±4.0	7, 12	6.0	0.95–1.00	...	7, 12
	145	18	14.5±4.0	7, 12	14.0	0.87–0.93	...	
	145	18	14.5±4.0	7, 12	33.5	...	0.59–0.63	
HD 36112 (MWC 758)..............	210±50	14	27±12	7, 14	38.9	...	0.53–0.67	7, 16
	210±50	14	27±12	7, 14	48.5	...	0.44–0.50	
HD 163296 (MWC 275).............	124±15	14	40±8	7, 12	7.0	0.87–0.98	...	7, 12, 19
	124±15	14	40±8	7, 12	12.5	0.83–0.91	...	
	124±15	14	40±8	7, 12	15.0	0.78–0.91	...	
	124±15	14	40±8	7, 12	34.9	...	0.42–0.50	
UX Ori	400±60	20	42.5±11.5	21	38.9	...	0.69	7
HD 31648 (MWC 480)..............	134±21	14	28±18	12, 14	12.5	0.90–0.95	...	12, 16
	134±21	14	28±18	12, 14	23.0	0.75–0.80	...	
	134±21	14	28±18	12, 14	38.0	...	0.41–0.55	
HD 150193 (MWC 863).............	134±21	14	28±18	7, 12	6.0	...	0.90–0.97	7, 12, 19
	134±21	14	28±18	7, 12	7.5	0.78–1.00	...	
	134±21	14	28±18	7, 12	12.5	0.70–0.85	...	
	134±21	14	28±18	7, 12	15.0	0.62–0.86	...	
	134±21	14	28±18	7, 12	17.5	0.75–0.78	...	
	134±21	14	28±18	7, 12	34.8	...	0.43–0.48	
AB Aur	147±20	14	51±14	14	7.5	0.90–0.95	...	12, 16, 19, 22, 23
	147±20	14	51±14	14	9.6	...	0.83–0.87	
	147±20	14	51±14	14	10.0	0.84–0.95	...	
	147±20	14	51±14	14	12.5	0.80–0.92	...	
	147±20	14	51±14	14	15.0	0.75–0.85	...	
	147±20	14	51±14	14	17.5	0.70–0.77	0.57–0.72	
	147±20	14	51±14	14	20.0	0.67–0.77	...	
	147±20	14	51±14	14	22.5	0.58–0.75	...	
	147±20	14	51±14	14	35.0	...	0.41	
	147±20	14	51±14	14	39.0	...	0.3	

TABLE 1—*Continued*

					VISIBILITY AVERAGES		
OBJECT NAMES	DISTANCE (pc)	DISTANCE REF.	LUMINOSITY ($L_\odot$)	LUMINOSITY REF.	Baseline (Mλ)	*H* Band	*K* Band	Visibility Ref.
Herbig Ae/Be Objects								
HD 344361 (WW Vul)	550	24	65±5	20	38.2	. . .	0.71–0.84	7
V1295 Aql (MWC 325, HD 190073)	290[a]	14	73±10	12, 14, 25	10.0	0.95–1.02	. . .	12, 16, 19, 26
	290[a]	14	73±10	12, 14, 25	14.0	0.87–0.92	. . .	
	290[a]	14	73±10	12, 14, 25	21.0	0.68–0.89	. . .	
	290[a]	14	73±10	12, 14, 25	37.0	. . .	0.42	
	290[a]	14	73±10	12, 14, 25	51.0	. . .	0.00–0.45	
T Ori	460	20	83	20	38.0	. . .	0.71–0.87	16
VV Ser	350±100	20, 27, 28, 29	43±20	20, 30	38.0	. . .	0.54–0.71	16, 22
	350±100	20, 27, 28, 29	43±20	20, 30	45.0	. . .	0.32–0.55	
V1578 Cyg (AS 477)	900	31	154±20	20	38.1	. . .	0.79–0.85	7
V1977 Cyg (AS 442)	700	32	300±210	7	38.3	. . .	0.30–0.95	7, 16, 22
	700	32	300±210	7	49.0	. . .	0.45–0.90	
MWC 419 (V594 Cas)	650	20	330	20	39.5	. . .	0.60–0.66	26
MWC 614 (HD 179218)	255±55	14	100±35[b]	12	11.0	0.65	. . .	12, 19, 26
	255±55	14	100±35[b]	12	14.0	0.62	. . .	
	255±55	14	100±35[b]	12	22.0	0.62	. . .	
	255±55	14	100±35[b]	12	40.0	. . .	0.0–0.45	
	255±55	14	100±35[b]	12	51.0	. . .	0.0–0.45	
MWC 120 (HD 37806)	360±130	14, 33	100±68	14, 33	38.0	. . .	0.35	16
LkHα 101	340[c]	34, 35	9000±5700[c]	34, 35	0.5	0.95–1.05	0.95–1.0	35
	340[c]	34, 35	9000±5700[c]	34, 35	1.0	0.85–0.95	0.85–0.95	
	340[c]	34, 35	9000±5700[c]	34, 35	1.5	0.75–0.85	0.65–0.75	
	340[c]	34, 35	9000±5700[c]	34, 35	2.0	0.60–0.70	0.45–0.55	
	340[c]	34, 35	9000±5700[c]	34, 35	2.5	0.45–0.55	0.30–0.40	
	340[c]	34, 35	9000±5700[c]	34, 35	3.0	0.30–0.40	0.15–0.25	
	340[c]	34, 35	9000±5700[c]	34, 35	3.5	0.20–0.30	0.05–0.15	
	340[c]	34, 35	9000±5700[c]	34, 35	4.0	0.15–0.25	. . .	
V380 Ori	445±15	20, 33	101±16	20, 36	11.0	0.96	. . .	19
	445±15	20, 33	101±16	20, 36	24.5	0.82–0.88	. . .	
MWC 147 (HD 259431)	800	20	6300	20	21.0	. . .	0.90	10, 19, 26
	800	20	6300	20	22.0	0.98	1.00	
	800	20	6300	20	23.5	1.00	. . .	
	800	20	6300	20	39.5	. . .	0.75–0.78	
	800	20	6300	20	50.0	. . .	0.71–0.76	
V1685 Cyg (MWC 340, BD +40 4124)	1000	20, 22, 37, 38, 39	5000±2000	20, 40	23.0	0.75–0.85	. . .	7, 16, 19, 22
	1000	20, 22, 37, 38, 39	5000±2000	20, 40	38.0	. . .	0.59–0.74	
	1000	20, 22, 37, 38, 39	5000±2000	20, 40	49.0	. . .	0.39–0.84	
MWC 297 (NZ Ser)	250±50	41	33000[d]±13000	12, 20, 41	7.5	0.86–0.92	. . .	12, 16, 19, 26, 42
	250±50	41	33000[d]±13000	12, 20, 41	10.0	0.81–0.97	. . .	
	250±50	41	33000[d]±13000	12, 20, 41	12.5	0.71–0.81	. . .	
	250±50	41	33000[d]±13000	12, 20, 41	15.0	0.67–0.70	. . .	
	250±50	41	33000[d]±13000	12, 20, 41	17.5	0.63–0.74	. . .	
	250±50	41	33000[d]±13000	12, 20, 41	20.0	0.50–0.67	. . .	
	250±50	41	33000[d]±13000	12, 20, 41	21.0	. . .	0.39–0.58	
	250±50	41	33000[d]±13000	12, 20, 41	39.0	. . .	0.00–0.45	
	250±50	41	33000[d]±13000	12, 20, 41	51.0	. . .	0.00–0.45	
MWC 1080	1600±600	20, 43	104000±76000	12, 20, 30	5.0	0.95–1.00	. . .	12, 16, 19, 22
	1600±600	20, 43	104000±76000	12, 20, 30	7.0	0.97–1.09	. . .	
	1600±600	20, 43	104000±76000	12, 20, 30	16.0	. . .	0.93–0.96	
	1600±600	20, 43	104000±76000	12, 20, 30	17.0	0.75–0.88	. . .	
	1600±600	20, 43	104000±76000	12, 20, 30	20.0	0.72–0.84	. . .	
	1600±600	20, 43	104000±76000	12, 20, 30	38.0	. . .	0.45–0.55	
MWC 166 (HD 53367)	1150	20	145000±95000	12, 20, 44	10.0	0.84–1.00	. . .	12, 19
	1150	20	145000±95000	12, 20, 44	12.0	0.87–0.92	. . .	
	1150	20	145000±95000	12, 20, 44	17.0	0.80–0.92	. . .	
Z CMa A	1100±50	13, 45, 46	333000±268000	47	27.4	. . .	0.42	7
	1100±50	13, 45, 46	333000±268000	47	29.0	. . .	0.43	

TABLE 1—*Continued*

OBJECT NAMES	DISTANCE (pc)	DISTANCE REF.	LUMINOSITY ($L_\odot$)	LUMINOSITY REF.	VISIBILITY AVERAGES			
					Baseline (Mλ)	H Band	K Band	Visibility Ref.
FU Ori Objects[e]								
FU Ori..	450	46	420±80	46, 48	9.6	. . .	0.88–1.01	49, 50
	450	46	420±80	46, 48	12.3	0.93–1.06	. . .	
	450	46	420±80	46, 48	15.9	. . .	0.94–1.03	
	450	46	420±80	46, 48	21.3	0.88–1.03	. . .	
	450	46	420±80	46, 48	38.6	. . .	0.86–0.95	
	450	46	420±80	46, 48	41.5	. . .	0.91–0.96	
	450	46	420±80	46, 48	47.5	. . .	0.80–0.89	
	450	46	420±80	46, 48	52.2	0.86–0.92	. . .	
	450	46	420±80	46, 48	63.2	0.89–0.93	. . .	
V1515 Cyg...	1000±200	46	175±75	46, 48	36.7	. . .	0.84–0.92	51
V1057 Cyg...	550±100	52	525±275	46, 48	38.5	. . .	0.77–0.89	26, 51
ZCMa SE...	1100±50	13, 45, 46	510±90	46, 48	26.3	. . .	0.40–0.42	51

[a] Only minimum values are known.

[b] Van den Ancker et al. (1998) suggest $316^{+272}_{-103}\ L_\odot$, but we adopt the most recent estimate of $100 \pm 35\ L_\odot$ by Monnier et al. (2006).

[c] Herbig et al. (2004) suggest 700 pc, but we use ~340 pc by Tuthill et al. (2002), who derived this distance from the analysis of the binary companion's apparent motion (luminosity scales with the distance).

[d] Significant differences in luminosity reported by different authors. We adopt values from Drew et al. (1997).

[e] The listed luminosities of FU Ori objects are dominated by accretion luminosity.

REFERENCES.—(1) Wichmann et al. 1998; (2) Akeson et al. 2005b; (3) Muzerolle et al. 2003; (4) Akeson et al. 2005a; (5) Chini 1981; (6) Eisner et al. 2005; (7) Monnier et al. 2005; (8) Colavita et al. 2003; (9) White & Ghez 2001; (10) Akeson et al. 2000; (11) Akeson et al. 2002; (12) Monnier et al. 2006; (13) Herbst et al. 1982; (14) van den Ancker et al. 1998; (15) Mannings & Sargent 1997; (16) Eisner et al. 2004; (17) Meeus et al. 2001; (18) Pérez et al. 2004; (19) Millan-Gabet et al. 2001; (20) Hillenbrand et al. 1992; (21) Hernández et al. 2004; (22) Eisner et al. 2003; (23) Millan-Gabet et al. 1999; (24) Friedemann et al. 1993; (25) Acke et al. 2005; (26) Wilkin & Akeson 2003; (27) Chavarria-K. et al. 1988; (28) de Lara et al. 1991; (29) Strom et al. 1974; (30) Acke & van den Ancker 2004; (31) Lada 1985; (32) Terranegra et al. 1994; (33) Warren & Hesser 1978; (34) Herbig et al. 2004; (35) Tuthill et al. 2002; (36) Testi et al. 1998; (37) Lorenzetti et al. 2002; (38) Shevchenko et al. 1991; (39) Strom et al. 1972; (40) van den Ancker et al. 2000; (41) Drew et al. 1997; (42) Malbet et al. 2007; (43) Levreault 1988; (44) Berrilli et al. 1992; (45) Claria 1974; (46) Hartmann & Kenyon 1996; (47) van den Ancker et al. 2004; (48) Sandell & Weintraub 2001; (49) Malbet et al. 2005; (50) Malbet et al. 1998; (51) Millan-Gabet et al. 2006a; (52) Straizys et al. 1989.

between the circumstellar environments of low- and high-L objects. Clustering is evident in low-L Herbig Ae/Be stars and T Tau stars, while high-L objects cluster at significantly larger scaled baselines (except for LkHα 101). The only exceptions are FU Ori objects, which appear more similar to high-L Herbig Be stars than to their older counterparts, T Tau stars. This suggests possible similarities in circumstellar geometry between these two types of objects. We address this issue in § 3.3.2.

Figure 2 indicates a slight difference between zones of T Tau clustering and low-L Herbig Ae/Be clustering. This is a result of differences in the stellar spectral shape, where T Tau stars contribute relatively more to the NIR flux than Herbig Ae/Be stars. How that influences the scaled visibility curves is more apparent in the next section, where we plot theoretical models over the data.

Trends in Figures 1 and 2 are so strong that we can use them to identify two anomalous individual cases:

1. *LkHα 101.*—Unlike other high-L objects, LkHα 101 shows a much smaller visibility with the scaled baseline, smaller even than low-L objects. This indicates a larger NIR-emitting area than in other YSOs. This object was one of the first YSOs imaged with the NIR interferometry (Tuthill et al. 2001), and it played an important role in establishing the existence of the inner disk clearing (Tuthill et al. 2002). Prior to the advent of NIR interferometry, the canonical model of the inner protoplanetary disk was a power-law accretion disk model. Images of LkHα 101 reconstructed from aperture masking interferometry data showed clearly that this object has a central clearing in the disk (Tuthill et al. 2002). The clearing was attributed to dust sublimation, and LkHα 101 became a prototype example of this new disk concept. Our scaled visibilities show that this object differs from other YSOs studied to date,

although the existence of inner clearing has been confirmed in other objects. It is possible that this object is indeed more similar to the low-L objects than high-L objects. There is a large uncertainty in the luminosity, distance, and evolutionary status of this object. Notice, however, that our scaled baseline in equation (1) is not affected by luminosity changes caused by changes in measured distance. There has to be an intrinsic error in luminosity to change the scaled baseline. For the most recent review of this object see Herbig et al. (2004).

2. *MWC 614.*—This object shows a flat visibility, which means that it is completely resolved at all used baselines. This indicates a much larger structure than other low-L objects. Monnier et al. (2006) suggest the possibility of a companion star at about 1″ distance, which would lead to an overestimate of the size of the emission region.

We excluded from this analysis objects that are most probably B[e] supergiants (MWC 349A, Danchi et al. 2001; Hofmann et al. 2002; MWC 342, Miroshnichenko & Corporon 1999; HD 45677, Monnier et al. 2006; de Winter & van den Ancker 1997; HD 58647, Monnier et al. 2005; Manoj et al. 2002). Their basic stellar parameters are shown in Table 2 and their scaled visibilities in Figure 3. When compared with YSOs, these objects do not fit into the clustering scheme recognized in Figures 1 and 2.

3. THEORETICAL INTERPRETATIONS

Clustering of scaled visibility indicates very similar images and hence presumably similar dust geometry. Variations in the model parameters should explain the cluster location, size, and shape. The advantage of modeling a cluster instead of individual objects is that here we can address the common properties of these types
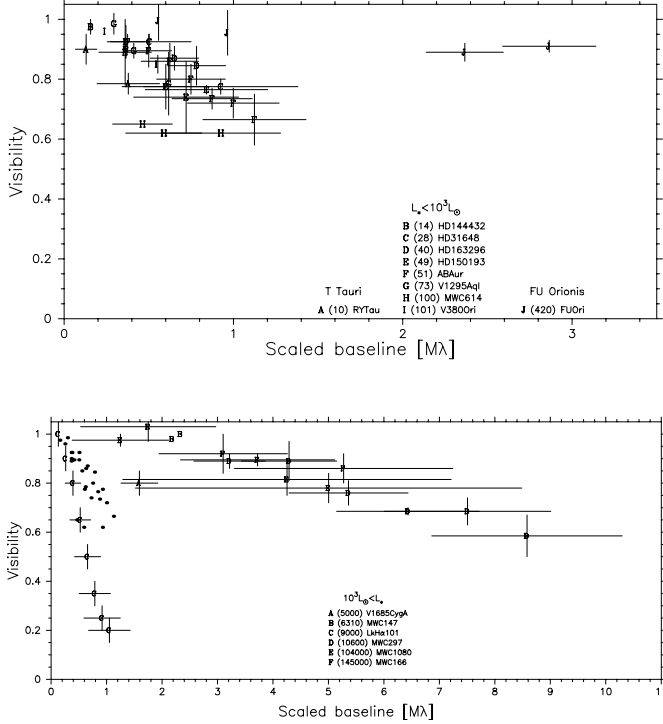
FIG. 1.—*H*-band visibility data with scaled baseline (see eq. [1]). Letters mark the averaged visibility data from Table 1. The vertical error bar is a scatter of measured visibility values, while the horizontal error bar derives from uncertainties in distance and luminosity. The top panel shows the data for a T Tauri star, Herbig Ae/Be stars of $L_\star < 10^3 \ L_\odot$, and FU Orionis. The bottom panel shows Herbig Be stars of $L_\star > 10^3 \ L_\odot$. Notice the tendency of low-luminosity stars (except for FU Ori) to cluster very compactly, which is a signature of very similar images of diffuse radiation, while high-luminosity stars have relatively small circumstellar structures. For comparison, dots in the bottom panel show the location of low-*L* stars. Stellar luminosities in units of $L_\odot$ are indicated together with the stellar name.

of objects without being misled by potential peculiarities of individual objects. We apply several different types of image models and discuss their constraints on the dust geometry based on fits to the data clusters.

3.1. *Uniform Brightness Ring*

A uniform brightness ring emerged as a prototype image model of NIR interferometry data. It assumes emission from a constant temperature disk with a central hole, which gives a ring of constant surface brightness. The inner radius of the ring is attributed to the dust sublimation, while the outer radius is derived from the total ring area required by the measured NIR photometric flux. Physical justification for this image configuration was found in the puffed-up inner disk model (Dullemond et al. 2001). The most recent NIR interferometry measurements of the image departures from centrosymmetry (Monnier et al. 2006) do not support the original version of the puffed-up model but prefer its more recent derivative by Isella & Natta (2005).

The visibility function for a uniform brightness ring (along its major or minor axis when inclined) combined with an unresolved star is (for details see Millan-Gabet et al. 2001; Eisner et al. 2004)

$$V_\lambda^{\rm ring}(B) = f_\lambda^\star + 2 \frac{1 - f_\lambda^\star}{\theta_2^2 - \theta_1^2} \left\{ \theta_2^2 \frac{J_1[\pi \theta_2 B(i)]}{\pi \theta_2 B(i)} - \theta_1^2 \frac{J_1[\pi \theta_1 B(i)]}{\pi \theta_1 B(i)} \right\},$$
(2)

$$B(i) = \begin{cases} B, & \text{major image axis}, \\ B \cos i, & \text{minor image axis}, \end{cases}$$
(3)

where J_1 is the Bessel function, $f_\lambda^\star$ is the fractional contribution of the stellar component to the total observed flux at the given NIR wavelength λ, i is the ring inclination angle, and θ_1 and θ_2 are the inner and outer ring size, respectively.

The inner ring radius θ_1 is controlled by dust sublimation and grain size. Cooling of smaller grains is less efficient than bigger grains; hence, bigger grains survive closer to the star. Vinković (2006) has shown analytically that in optically thick disks made of a mixture of grain sizes, the inner radius is dictated by the largest grains in the mix. They provide shielding of smaller grains from direct stellar radiation, which allows smaller grains to move closer to the star. The inner disk radius of optically thick disks is, therefore, controlled by the largest grains, that is, by their sublimation. The most efficient cooling in NIR is archived by big (micron size or larger) grains because of their gray opacity in NIR and shorter wavelengths. For that reason, big grains reach the minimal possible dust distance from the star. Mid-infrared spectroscopy of YSOs shows that the presence of big grains is a typical feature of circumstellar dust in these objects (e.g., van Boekel et al. 2003; Przygodda et al. 2003; van Boekel et al. 2005). Thus, the inner disk radius in YSOs is uniquely defined by gray dust grains.

On the other hand, dust sublimation does not provide a unique solution to the inner radius of protoplanetary disks because we lack constraints on the exact density structure of these disks. Dust dynamics, growth, and sublimation can make the innermost part of the disk vertically optically thin and allow more efficient cooling of the disk. This reduces the local diffuse radiation and enables the optically thin zone of the inner disk to extend much closer to the star than the optically thick part of the disk. Hence, the inner disk radius due to gray dust of temperature T_D is (Vinković 2006)

$$R_{\rm in} = 0.0344 \Psi \left(\frac{1500 \ {\rm K}}{T_D} \right)^2 \sqrt{\frac{L_\star}{L_\odot}} \quad ({\rm AU}),$$
(4)

where Ψ depends on the details of the disk structure and radiative transfer and can be as low as $\Psi \sim 1.2$ for optically thin inner disks or the maximum of $\Psi = 2$ in the case of entirely optically thick disks. In objects with a nonnegligible accretion, $L_\star$ should be replaced with $L_\star + L_{\rm acc}$. The scaled baseline (eq. [1]) is introduced from equation (4) by considering the disk size at 1 pc and $1 \ L_\odot$,

$$\theta_1 = 0.0688 \Psi \left(\frac{1500 \ {\rm K}}{T_D} \right)^2 \quad ({\rm arcsec}).$$
(5)

The stellar size $\theta_\star$ follows directly from $L_\star$, while the outer disk size θ_2 is derived from the requirement of the total flux being a sum of the stellar and ring components [i.e., $V_\lambda(B = 0) = 1$],

$$\theta_2^2 = \theta_1^2 + \frac{1 - f_\lambda^\star}{f_\lambda^\star \cos i} \frac{\mathfrak{B}_\lambda(T_\star)}{\mathfrak{B}_\lambda(T_D)} \theta_\star^2,$$
(6)

where $\mathfrak{B}_\lambda$ is the Planck function and $T_\star$ is the stellar temperature. Now we can explore the range of parameter values constrained by the visibility clusters. We do not discuss this model for high-*L* objects because no satisfactory fit is possible.

3.1.1. *Inclination*

The clusters are expected to spread in size because of randomization of observed disk inclinations. With equation (2) we address only the major and minor axes, which are the image extremes,
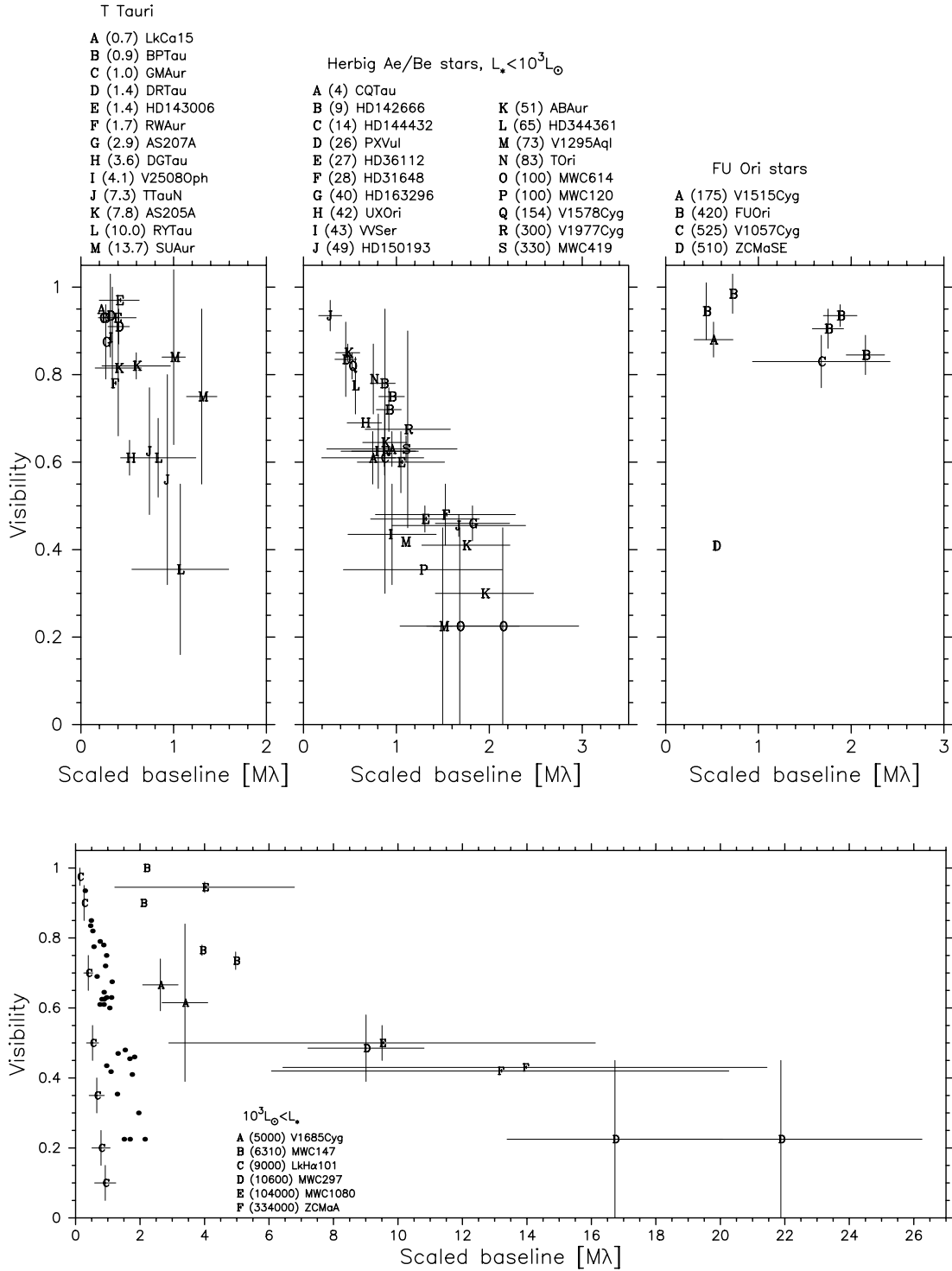
T Tauri

A (0.7) LkCa15
B (0.9) BPTau
C (1.0) GMAur
D (1.4) DRTau
E (1.4) HD143006
F (1.7) RWAur
G (2.9) AS207A
H (3.6) DGTau
I (4.1) V2508Oph
J (7.3) TTauN
K (7.8) AS205A
L (10.0) RYTau
M (13.7) SUAur

Herbig Ae/Be stars, $L_* < 10^3 L_\odot$

A (4) CQTau
B (9) HD142666
C (14) HD144432
D (26) PXVul
E (27) HD36112
F (28) HD31648
G (40) HD163296
H (42) UXOri
I (43) VVSer
J (49) HD150193

K (51) ABAur
L (65) HD344361
M (73) V1295Aql
N (83) TOri
O (100) MWC614
P (100) MWC120
Q (154) V1578Cyg
R (300) V1977Cyg
S (330) MWC419

FU Ori stars

A (175) V1515Cyg
B (420) FUOri
C (525) V1057Cyg
D (510) ZCMaSE

$10^3 L_\odot < L_*$

A (5000) V1685Cyg
B (6310) MWC147
C (9000) LkHα101
D (10600) MWC297
E (104000) MWC1080
F (334000) ZCMaA

Fig. 2.—Same as Fig. 1, but for *K*-band data. T Tauri, Herbig Ae/Be, and FU Orionis are now separated for clarity into their own panels. The clustering of low-luminosity objects and their distinction from high-luminosity objects are clearly visible. The clustering is even more evident as we parameterize the data by various visibility functions (see Figs. 4–11).

TABLE 2
B[e] STARS

Object	Distance (pc)	Distance Ref.	Luminosity ($L_\odot$)	Luminosity Ref.	Visibility Ref.
HD 58647	295±65	1	295±50 (2)	2	2
HD 45677	1000±500	3	14000±7000	4	4
MWC 349A	1200	5	55000±25000	5, 6	6, 7
MWC 342	1000	8	31500±16500	4, 8	4

REFERENCES.—(1) van den Ancker et al. 1998; (2) Monnier et al. 2005; (3) de Winter & van den Ancker 1997; (4) Monnier et al. 2006; (5) Cohen et al. 1985; (6) Danchi et al. 2001; (7) Hofmann et al. 2002; (8) Miroshnichenko & Corporon 1999.
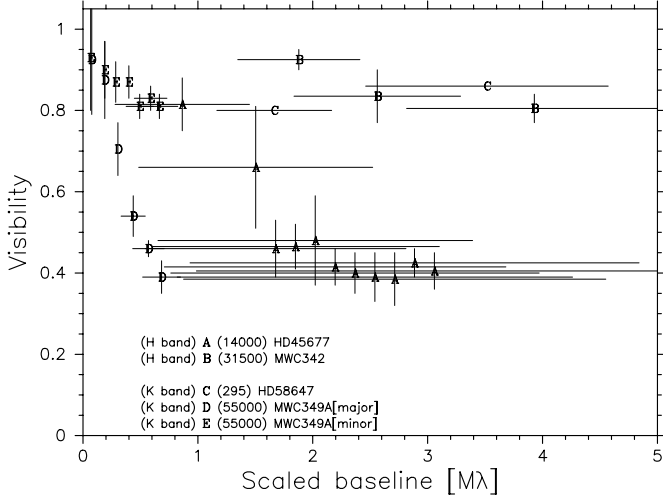
Fig. 3.— Objects that are most probably B[e] stars with infrared excess and erroneously classified as YSOs in observational campaigns. This figure shows how they also differ from YSOs in their scaled visibility (see Figs. 1 and 2). Images of MWC 349A are reconstructed from aperture masking interferometry, and here we show the visibility along its major and minor image axes.

while the orientation of baselines can exist in between these two position angles. Nonetheless, observations are usually performed within a range of position angles, which increases the chance of covering the image extremes. These scans of position angles are usually incorporated in the visibility vertical error bars.

We apply equation (2) to the low-L Herbig Ae/Be cluster and T Tauri cluster. We use the dust sublimation temperature of 1500 K and the optically thick disk of $\Psi = 2$. The stellar temperatures are 10,000 K for Herbig stars and 5000 K for T Tau

stars. The fraction of stellar flux $f^\star$ at different wavelengths depends on spectral shapes of stellar and diffuse radiation. Instead of letting this be a free parameter, we use observed spectral energy distributions (SEDs) of YSOs to constrain its value. This way we actually fit the observed diffuse flux level (relative to the stellar flux level), which is needed for realistic modeling of both the circumstellar geometry and the SEDs. Observations show that the fraction of stellar flux in low-L Herbig Ae/Be stars is in the range $f^\star \sim 0.2-0.6$ in H band and $f^\star \sim 0.1-0.3$ in K band (Millan-Gabet et al. 2001; Vinković et al. 2006), while for classical T Tauri stars it is $f^\star \sim 0.3-0.7$ in K band (Cieza et al. 2005). Therefore, we choose medium values of 0.4, 0.2, and 0.5, respectively.

Comparison of models with the data is shown in Figure 4. Herbig Ae/Be clusters are nicely reproduced with this model for the range of inclination angles between $0°$ and $60°$. The model fails in the T Tau cluster. These objects appear larger than expected from the model, and only unrealistically small (i.e., inconsistent with observations) values of $f^\star = 0.1-0.2$ can reproduce the cluster size. This is consistent with the findings of Akeson et al. (2005b), who performed a similar study and concluded that some T Tau stars appear bigger than the expected dust sublimation radius. There is also no positive correlation between size and accretion; on the contrary, the opposite trend (decreasing size with increasing contribution of accretion luminosity) has been reported by Akeson et al. (2005b). Hence, we conclude that this model cannot provide a satisfactory explanation of the T Tau data cluster, and we continue with only addressing model parameters in low-L Herbig Ae/Be stars.

Interestingly enough, the inclination angles up to $60°$ are sufficient to explain the low-L cluster size even though we have not yet varied other parameters. Since we expect other parameters to spread the model further, this might be an indication of images appearing as if they had inclination angles in a smaller range
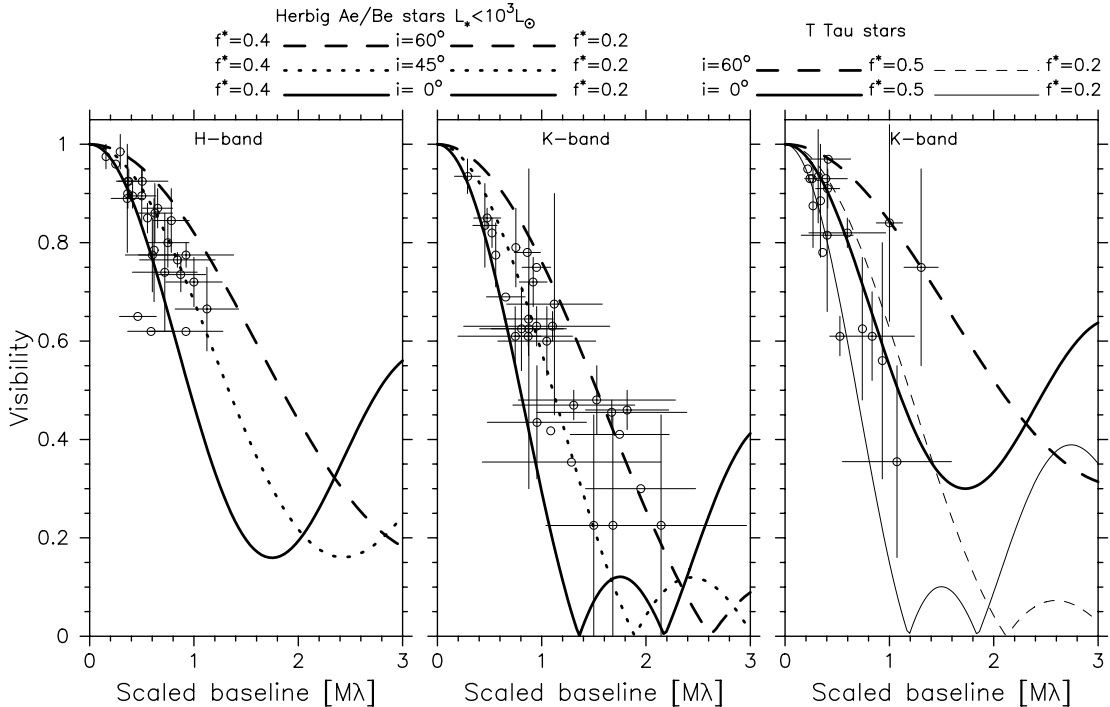
Fig. 4.—Visibility models of inclined uniform brightness ring. The data are the same as in Figs. 1 and 2. The models assume the ring temperature $T_D = 1500$ K and $\Psi = 2$ in eq. (5) and $T_\star = 10,000$ K for Herbig Ae/Be stars and $T_\star = 5000$ K for T Tauri stars. The fraction of the stellar flux $f^\star$ is set to typical values: 0.4 in H band and 0.2 in K band for low-L Herbig Ae/Be stars and 0.5 in K band for T Tauri stars. While these values reproduce the shape and spread of the low-L clusters, T Tau stars appear larger than the model. An unrealistically low value of $f^\star = 0.2$ is needed for T Tau stars.
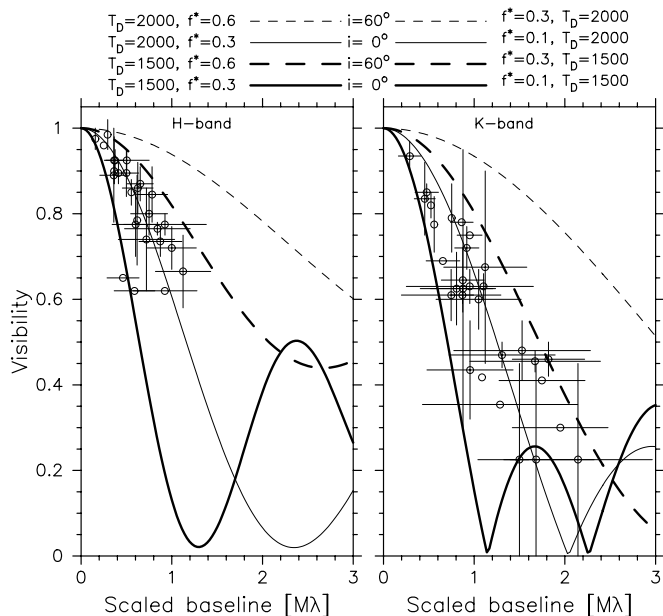
Fig. 5.—Low-*L* Herbig Ae/Be stars modeled with inclined uniform brightness ring. The model parameters are the same as in Fig. 4, except for the stellar fraction $f^\star$ and ring temperature T_D. The stellar flux fraction covers the lower and upper limits, combined with the lower and upper inclination angle limits from Fig. 4. Data clusters appear smaller than the range of these parameters and with a clear preference for dust temperatures of 1500 K. The T Tau *K*-band cluster cannot be successfully fitted with this model (see Fig. 4).

than expected from random orientations. We address this issue further below.

3.1.2. *Stellar Flux Fraction and Dust Sublimation*

Next we explore the above-mentioned limits in the stellar flux fraction. Figure 5 shows models with limiting values of $f^\star$ combined with disk inclinations. Combining low $f^\star$ with low *i* and high $f^\star$ with high *i* brings up extremes in visibility functions. Comparison with the data shows that clusters appear slightly more compact than these limits, but this could be just the result of a small data set. However, freedom in choosing the disk temperature (i.e., dust sublimation temperature) results in large model deviations from the data, as shown in Figure 5. The temperature of 2000 K is often suggested to explain the data in some individual objects, but when it comes to explaining the collective data set, the temperature of 1500 K emerges as the most plausible choice, assuming that visibility data clusters are indeed a result of very similar physical conditions in all these objects.

3.1.3. *Stellar Temperature and Disk Opacity*

Objects comprising the data clusters have a range of stellar temperature from 7500 to 12,000 K for low-*L* Herbig Ae/Be stars. Figure 6 shows how this spread in temperature affects the model. Since the stellar spectrum at these temperatures peaks at wavelengths shorter than NIR, changes in the stellar temperature do not have a significant effect on the NIR images. Differences of these models from the 10,000 K models in Figure 5 are small, and conclusions from § 3.1.2 also hold here.

In addition, we explore the possibility of an optically thin inner disk and apply $\Psi = 1.2$ to these models. Figure 7 shows that optically thin disks would be an option if disks are almost face-on, but not when the whole cluster of visibility data is considered. Since $\Psi \sim 1.2$ is the minimal possible value, maybe some inter-

mediate $(1.2 \lesssim \Psi < 2)$ values exist. However, the NIR excess in Herbig Ae/Be stars cannot be explained by optically thin disks alone. Instead, an additional circumstellar structure, such as a puffed-up disk or a dusty halo, has to be invoked to reproduce the observed amounts of NIR flux (Vinković et al. 2006).

3.2. *Dusty Halo*

An alternative model to disk geometries is a dusty halo around the disk inner regions. Compact (~10 AU) optically thin halos have been invoked to explain the NIR spectrum of Herbig Ae/Be

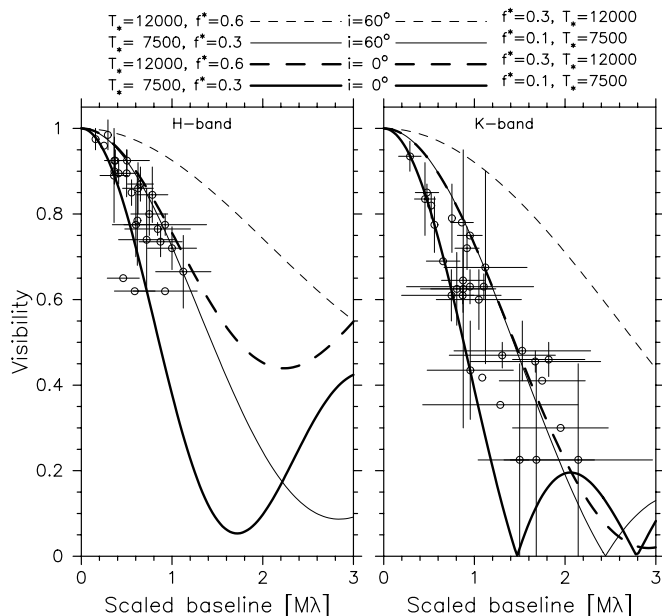Fig. 6.—Same as Fig. 5, but for different stellar temperatures. The disk temperature is set to 1500 K.

Fig. 7.—Same as Fig. 5, but now for optically thin disks with $\Psi = 1.2$. Although the model of an optically thin disk would work for small inclination angles, the data clusters clearly support an optically thick disk when a full range of inclination angles is considered.
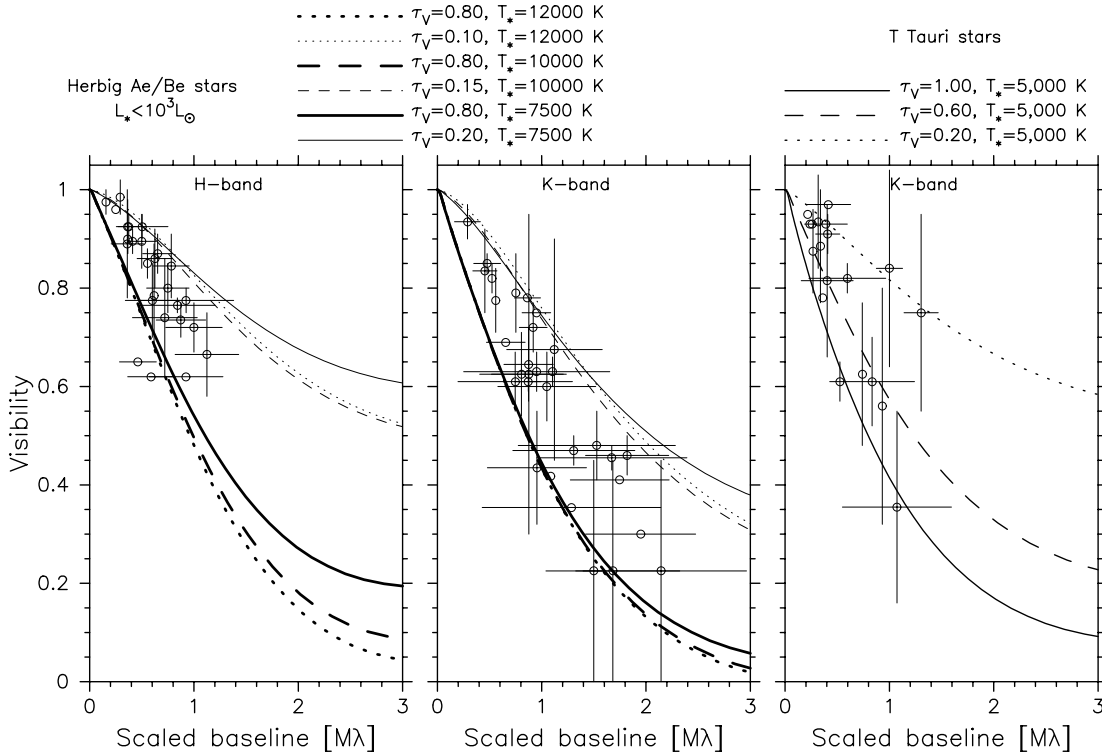
FIG. 8.—Visibility models of dusty halos. The models assume a spherical halo for simplicity. The dust is 1 μm silicate grains sublimating at 1500 K. Lines show visibility functions for various optical depths and stellar temperatures. Optically thin halos are sufficient to explain the data clusters.

stars and their NIR visibility (Johns-Krull & Valenti 2001; Vinković et al. 2006). The exact physical mechanism for creating such a halo is not known, but the variability of YSOs (discussed in § 4.2) supports its existence as a dusty outflow.

In its most rudimentary form, the halo can be approximated with a spherical geometry. We emphasize that this is just a convenient approximation, while a more realistic description of a dusty outflow probably requires a flattened and clumpy halo. Nevertheless, optically thin halos are dominated by direct stellar heating and, therefore, will maintain similar temperature profiles, no matter the exact geometry. We can also ignore the disk heating of the halo because optically thin halos are transparent to the disk emission. The exact images of the disk and halo model ultimately depend on detailed properties of the halo and the intrinsic ratio between the disk and halo surface brightness. These images also depend on the inclination angle, which is something that we cannot address here with our simple approximation. We caution that halo models cannot be dismissed by postulating that they should produce centro-symmetric images (e.g., Isella et al. 2006). Speckle interferometry images of the Herbig Be star R Mon are an illustrative example of complicated asymmetric images produced by a parabolic dusty out-flow combined with the inclined disk (Weigelt et al. 2002).

The halo radiative transfer is solved with the code DUSTY (Ivezić et al. 1999[1]), which takes advantage of the scaling properties of the radiative transfer problem for dust absorption, emission, and scattering (Ivezić & Elitzur 1997). The stellar spectra used in our modeling are taken from Kurucz models. The silicate dust optical constants are from Dorschner et al. (1995) ($x = 0.4$ olivine). The radial density profile is described with r^{-2} since Vinković et al. (2006) showed that it can reproduce the NIR SEDs of Herbig Ae/Be stars. The outer halo radius has to be large enough

to extend beyond the distance where the halo brightness drops below interferometric or photometric detection. Hence, we fix it to be 100 sublimation radii. Visibility functions at specified wavelengths are part of the computational output from the code. The output visibility already has the stellar and diffuse components included; thus, we do not need to specify $f^\star$ in this modeling. The variable that indirectly controls the amount of diffuse flux in optically thin halos is the radial optical depth (see Appendix in Vinković et al. 2003).

The provided spatial frequency q_{dusty} from DUSTY is the frequency scaled with the angular size of the inner cavity (Ivezić & Elitzur 1996). Since the inner cavity radius r_1 for $L_\star = 10^4 \, L_\odot$ is also provided in the output, we can derive the scaled baseline from

$$B_{\text{scaled}} = 1.54 \times 10^{14} q_{\text{dusty}} \left(\frac{r_1}{\text{cm}}\right)^{-1} \left(\frac{\lambda}{\mu\text{m}}\right). \quad (7)$$

Comparison between halo visibility models and data clusters is presented in Figure 8. Dust grains used in the models are 1 μm in size and sublimating at 1500 K. We use stellar temperatures typical for these stars and find that optically thin halos can explain the data clusters. The required visual optical depth in low-L Herbig Ae/Be stars is $\tau_V \sim 0.15$–0.8, which is in agreement with $\tau_V \gtrsim 0.2$ derived from fits to SEDs (Vinković et al. 2006). The T Tau cluster displays a slightly larger upper optical depth limit of $\tau_V \sim 1$.

The grain size of $\sim 1 \, \mu$m seems optimal to fit the data. Figure 9 shows how the visibility changes when the grain size is reduced to 0.2 μm or increased to 10 μm. These changes are caused by variations in the sublimation radius R_{in} of the halo, where larger grains reduce and smaller grains increase this radius. Similar grain sizes fitting the data mean that the inner halo radii are also very similar.
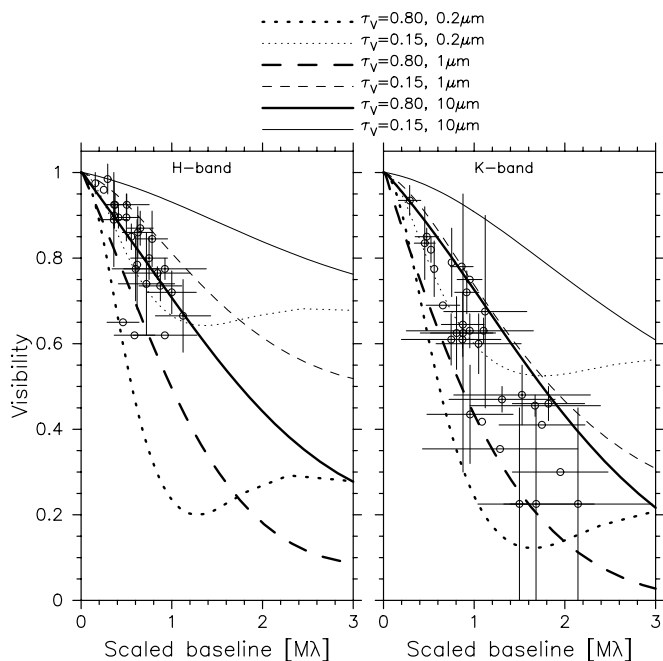
---

[1] Accessible at http://www.pa.uky.edu/~moshe/dusty.

FIG. 9.—Same as Fig. 8, but now for different grain sizes. The data clusters belong to low-L Herbig Ae/Be stars. The model stellar temperature is 10,000 K. Lines show variations in optical depth and grain size. If dusty outflows exist in these objects, then the visibility data suggest a dust grain size of $\sim 1 \ \mu$m.

The model is unsuccessful in explaining the visibility of high-L Herbig Be stars. The only way to reach the observed visibility levels of these stars is to keep the halo at tiny optical depths, which creates a flat visibility due to an unresolved star at observational baselines. This was the approach used by Vinković et al. (2006) in fitting one high-L star (MWC 297). Since observed visibilities show a nonflat structure, this model is unsatisfactory. This shows that if the halo model is correct in low-L objects, then high-L objects differ from low-L objects by not having a dusty halo, which is not surprising considering that large luminosities would impose a large radiation pressure on optically thin dusty halos. Such a scenario would be in agreement with observations showing that YSOs of spectral type earlier than about B5 disperse their circumstellar environment much faster than later spectral types (Fuente et al. 1998). Hence, the NIR visibilities of high-L objects imply that these are stars that are still surrounded by circumstellar gas and dust, but the process of dispersal has already started within their immediate environment.

3.3. Accretion Disks

Prior to the discovery of inner disk holes in low-L Herbig Ae/Be stars produced by dust sublimation (Monnier & Millan-Gabet 2002), accretion disks were assumed to be the main source of the NIR excess in YSOs. Since accretion disks extend closer to the star than the dust sublimation radius, they are still a favored explanation for the NIR visibility data of high-L Herbig Be stars (Malbet et al. 2007; Monnier et al. 2005; Eisner et al. 2003, 2004; Monnier & Millan-Gabet 2002; Millan-Gabet et al. 2001).

3.3.1. Accretion Disk Model

The total luminosity of stars with accretion disks is a sum of the stellar and the accretion luminosities, $L_{\rm tot} = L_\star + L_{\rm acc}$, where $L_{\rm acc} = GM_\star \dot{M}_{\rm acc}/2R_\star$. Combining stellar heating (Friedjung 1985; for $R \gtrsim 2R_\star$) and viscous heating (Lynden-Bell & Pringle 1974)

of a geometrically thin, optically thick disk results in the disk temperature

$$T(\theta) = \left[2.19 \times 10^{-7} \left(\frac{R_\star}{R_\odot} \right)^3 T_\star^4 + 4.21 \times 10^{16} \left(\frac{M_\star}{M_\odot} \right) \right.$$
$$\left. \times \left(\frac{\dot{M}_{\rm acc}}{M_\odot \ {\rm yr}^{-1}} \right) \left(1 - \sqrt{\frac{\theta_{\rm in}}{\theta}} \right) \right]^{1/4} \left(\frac{L_{\rm tot}}{L_\odot} \right)^{-3/8} \theta^{-3/4}, \quad (8)$$

where θ is the *scaled* angular size derived from the disk radius R and the total luminosity

$$\theta = 2\sqrt{\frac{L_\odot}{L_{\rm tot}}} \frac{R}{1 \ {\rm AU}}. \quad (9)$$

The inner disk edge size $\theta_{\rm in}$ (radius $R_{\rm in}$) and disk inclination angle i are free parameters. The stellar fraction of NIR flux $f_\lambda^\star$ can be computed by integrating the disk emission

$$\frac{1}{f_\lambda^\star} - 1 = \frac{2\cos i}{\theta_\star^2 \mathfrak{B}_\lambda(T_\star)} \int_{\theta_1}^{\theta_{\rm out}} \mathfrak{B}_\lambda[T(\theta)]\theta \, d\theta, \quad (10)$$

where the upper integral limit can be any size where the disk temperature drops below detection at NIR wavelengths.

The visibility is a sum of narrow rings over the disk surface. Each ring has the visibility described by equation (2); hence, the accretion disk visibility is

$$V_\lambda^{\rm acc}(B) = f_\lambda^\star \left(1 + 2\cos i \sum_{\theta_1}^{\theta_{out}} \frac{\mathfrak{B}_\lambda[T(\theta)]}{\mathfrak{B}_\lambda(T_\star)} \right.$$
$$\times \left\{ \frac{(\theta + \Delta\theta)^2}{\theta_\star^2} \frac{J_1[\pi(\theta + \Delta\theta)B(i)]}{\pi(\theta + \Delta\theta)B(i)} - \frac{\theta^2}{\theta_\star^2} \frac{J_1[\pi\theta B(i)]}{\pi\theta B(i)} \right\} \right), \quad (11)$$

where $\Delta\theta$ is a small angular step and $B(i)$ is the scaled baseline defined in equation (3).

Unlike in dust ring models, here we do not have a firm theoretical limit on the inner radius $R_{\rm in}$, but if the disk accretes onto the star, then the inner radius of several stellar radii is expected. The main problem in constraining these models is that precise stellar parameters are not well known for high-L Herbig Be stars. On top of that, accretion luminosities are relatively small compared to stellar luminosities, which makes accretion rates difficult to constrain.

All these uncertainties are illustrated in Figure 10, where we compare various accretion disk models with the data (we ignore anomalously low visibilities of LkHα 101 in this discussion, as described in § 2). We display models with no accretion (a purely reprocessing disk) and with a very high accretion rate of $10^{-4} \ M_\odot \ {\rm yr}^{-1}$ to illustrate how models with almost any accretion rate can be built to fit the visibility data (for further discussion see, e.g., Malbet et al. 2007). Models are calculated only for face-on inclination, since any loss of flux in inclined disks can be compensated by an increased inner disk radius (Millan-Gabet et al. 2001). Also, inclination increases the visibility, which again calls for a larger inner radius to fit the data. Hence, presented models put a lower limit on $R_{\rm in}$.

3.3.2. The Nature of Disks in High-L Herbig Be Stars

It seems that some models with $R_{\rm in} \sim 5R_\star$ can fit the visibility, which would be in agreement with the magnetic accretion radii
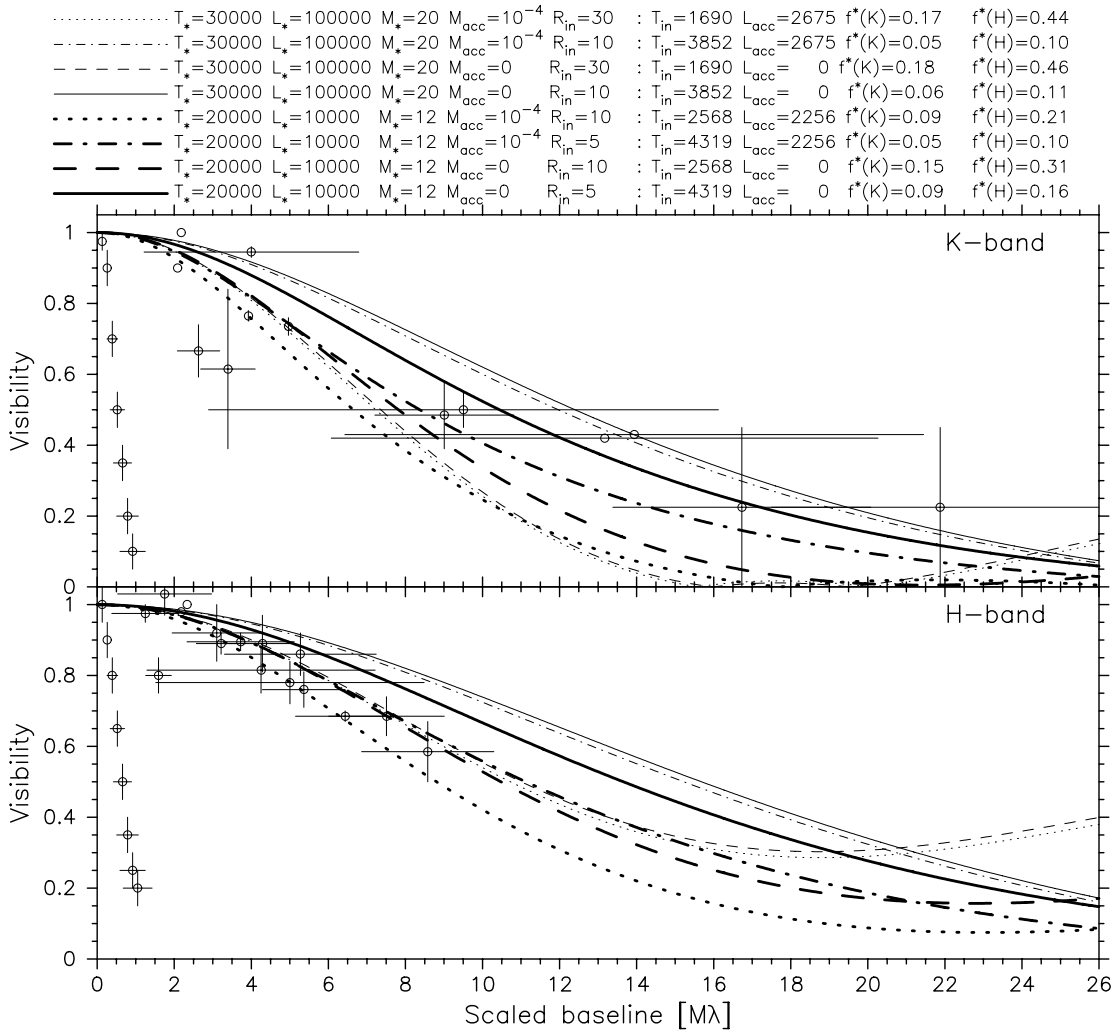
Fig. 10.—Accretion disk models of high-L Herbig Be stars. The data are the same as in Figs. 1 and 2. The legend lists parameter values used in modeling: stellar temperature $T_\star$ in K, stellar luminosity $L_\star$ and mass $M_\star$ in solar units, accretion rate $\dot{M}_{\rm acc}$ in $M_\odot$ yr^{-1}, and inner disk radius $R_{\rm in}$ in solar units. Presented models are for face-on disks. Other listed parameters are derived from the model: disk temperature $T_{\rm in}$ in K at the inner disk edge, accretion luminosity $L_{\rm in}$ in solar units, and stellar flux fraction in K band [$f^\star(K)$] and H band [$f^\star(H)$]. See § 3.3 for more details.

implied from T Tau stars (Kenyon et al. 1996). However, Figure 10 shows that models with $\gtrsim 10 R_\star$ are also applicable. Moreover, a detailed modeling of MWC 297 yields $R_{\rm in} \sim 17 R_\star$ (Malbet et al. 2007), which raises the question of what is the physical process that truncates the disk at these radii.

Monnier et al. (2005) suggest that the NIR visibility of high-L objects is due to dust in the accretion disk. In that case the inner radius is dictated by the dust sublimation temperature. Figure 10 shows that sublimation temperatures would require $R_{\rm in} \gtrsim 20$. Such disks would be optically thick in their purely gaseous part inside of the dusty disk hole. This would allow shielding of the dust from direct stellar radiation, so that the dust can move closer to the star than the ordinary dust sublimation distance. The extent of this shielding can be estimated by scaling the high-L visibility clusters in Figures 1 and 2 to the location of low-L clusters. We find that all the stellar flux shorter than ~ 0.6 μm has to be removed to make this process work. The obtained scaling factor is ~ 7, which also shows how smaller high-L objects are from the dust sublimation size typical of low-L objects.

Optically thin gas can be optically thick in some molecular and atomic lines, but it would be transparent at other wavelengths and incapable of producing such a severe reduction of the stel-

lar flux. The shielding is, therefore, plausible only if the gas is completely optically thick, which also implies high accretion rates ($\gtrsim 10^{-7} M_\odot$ yr^{-1}; Muzerolle et al. 2004; Bell & Lin 1994; Hartmann et al. 1993). On the other hand, this creates a problem because the side effect is a strong NIR radiation that can actually overshine the dusty disk. Muzerolle et al. (2004) demonstrate this in the case of a puffed-up dusty disk, where gas emission from accretion disks of $\dot{M}_{\rm acc} \gtrsim 10^{-6} M_\odot$ yr^{-1} would dominate the NIR. Since shielded dusty accretion disks do not have such a puffing, their NIR dust emission is smaller than from puffed-up disks and, therefore, competes with smaller accretion rates.

The effect is even more pronounced in NIR visibilities where a bright optically thick gas would affect images by decreasing the observed inner disk radius. Comparison between disk models of different inner radii in Figure 10 shows that any such decrease would significantly alter the visibilities. Thus, if dust is the source of NIR visibility of high-L objects, then the gas inside of the dust sublimation radius has to be optically thick for stellar radiation, but not bright in the NIR at the same time. Scattering of UV by low-density gas was suggested by Monnier & Millan-Gabet (2002) as a possible solution, but this cannot work because (1) large optical depths are needed to block almost all of the scattered stellar

flux, and (2) even if all of the stellar UV flux is removed, it is still not enough to make high-L scaled visibilities similar to low-L visibilities. This dilemma of how to reconcile such properties of the gaseous disk within the dust sublimation zone is actually quite old, and it was already recognized in a slightly different context by Hartmann et al. (1993).

It is, therefore, possible that instead of dust, the NIR flux of high-L objects originates from gas emission despite confusion about the inner disk radius. This would suggest that these stars have high accretion rates and their circumstellar environment is evolutionary similar to FU Ori objects (young counterparts of T Tau stars). Since both types of objects are of a similar age, they probably share similarities in the accretion process. Fast pre–main-sequence (PMS) evolution of massive stars actually requires high accretion rates (Palla & Stahler 2000). Also, observed high mass-loss rates imply high accretion rates in massive stars (Cesaroni et al. 2007; Shepherd & Churchwell 1996), similar to massive winds supported by high accretion rates in FU Ori stars (Sandell & Weintraub 2001; Calvet et al. 1993). The main difference is the ability of highly luminous Herbig Be stars to relatively quickly disperse their circumstellar matter (Fuente et al. 1998).

The standard viscous disk model predicts proportionality between the disk mass and the accretion rate (e.g., Calvet et al. 2000). Thus, high accretion rates would suggest higher disk masses in high-L than in low-L objects. Observations, however, show exactly the opposite (Fuente et al. 2003). It may be that the dispersion of circumstellar matter around high-L stars starts with disk erosion due to disk and stellar winds. This may reduce the disk mass and explain the observed decrease in disk masses. Their destructive nature may also explain why these stars form a data cluster at ~7 times larger scaled baselines than low-L YSOs instead of producing a range of values due to disk optical depth variations between objects. Namely, it may be that only high-density and high-accretion disks can survive so close to these luminous stars, which would result in disks with very similar NIR signatures.

High accretion rates may also be implied from the recently observed correlation between the accretion rate and the square of the stellar mass of low-L YSOs (e.g., Calvet et al. 2004; Muzerolle et al. 2005; Garcia Lopez et al. 2006; Natta et al. 2006 and references therein). If this correlation is not just a selection effect (Clarke & Pringle 2006), then it probably extends to high-L objects, too. The required accretion rates would be $\dot{M}_{acc} \gtrsim 10^{-7}\ M_\odot\ yr^{-1}$, which is exactly what we suggest based on the NIR visibilities.

There are additional complications in deducing the nature of disks around Herbig Be stars. MWC 166 is, for example, a binary with a mean distance of ~1.7 AU between components and an orbital eccentricity of $e = 0.28$ (Pogodin et al. 2006). The binary is surrounded by a common gaseous envelope, and the existence of the disk in this system is a more puzzling problem than our general discussion about Herbig Be stars. We also ignore any contribution from the NIR free-free emission. Although this is a good approximation for Herbig Be stars, it is possible that some objects have a significant amount of free-free emission (e.g., MWC 297; Porter et al. 1998)

3.3.3. *FU Ori Accretion Disks*

Accretion disks in FU Ori stars are corroborated with NIR visibility measurements, as evident from Figure 11, where we compare the visibility data of FU Ori stars and accretion disk models. Modeling is simplified in this case due to similarities in stellar properties of FU Ori stars. We use face-on disks and stellar temperature, mass, and luminosity of 5000 K, 1 $M_\odot$, and 4 $L_\odot$, respectively. Classical accretion disks of $R_{in} = 3R_\star$–$5R_\star$ and $\dot{M}_{acc} = 10^{-4}$ to $10^{-5}\ M_\odot\ yr^{-1}$ reach the upper observed visibility levels
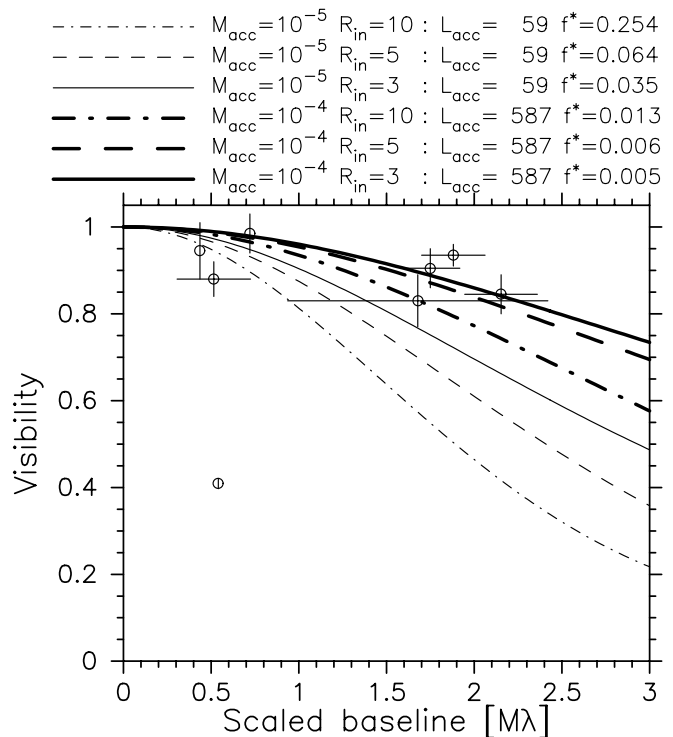

FIG. 11.—Same as Fig. 10, but for FU Ori stars. The K-band data are shown. The stellar temperature, mass, and luminosity are 5000 K, 1 $M_\odot$, and 4 $L_\odot$, respectively. Lower than expected visibilities are most probably an indication of overresolved large dusty halos (Millan-Gabet et al. 2006a).

(see also Malbet et al. 1998, 2005; Millan-Gabet et al. 2006a). There is a problem with anomalously low visibility of Z CMa SE, which is more consistent with T Tau visibilities. Other FU Ori stars also show a slightly smaller visibility than expected from pure accretion disks, which indicates an additional larger completely resolved circumstellar structure. Millan-Gabet et al. (2006a) argue that this is due to a large dusty envelope. Such a disk+envelope structure was previously predicted from the overall infrared SED (Hartmann & Kenyon 1996). This configuration and derived accretion rates were recently confirmed by modeling the infrared spectra of FU Ori stars taken with the *Spitzer Space Telescope* (Green et al. 2006). However, Quanz et al. (2006) modeled their mid-IR visibilities of FU Ori without any additional structure such as a dusty envelope and concluded that the presence of an accretion disk is sufficient to explain this object.

4. DISCUSSION

4.1. *The Importance of Dust Dynamics*

We usually approach this kind of study with the assumption that circumstellar environments of YSOs share enough similarities to be successfully described with one universal theoretical model. This is a very strong assumption considering that the spectra reveal very dynamic gaseous disks around YSOs (e.g., Mora et al. 2004). Since gravity and gas drag are two forces that dictate dust dynamics within protoplanetary disks, dust should also display a very dynamic behavior. The infrared spectra provide evidence that this is indeed the case: the mid-IR dust features exhibit clear signatures of small grains in the disk surface (Acke & van den Ancker 2004), which is possible only if dust dynamics persistently replenishes the surface with these grains (Dullemond & Dominik 2005).

Dust dynamics is, however, ignored when it comes to formulating dusty disk models used in calculating synthetic infrared spectra

and images. The disk is modeled with a smooth surface that seemingly appears dynamically passive. This is a good approximation when it comes to modeling data taken at one epoch, but multi-epoch data reveal that YSOs are far more complicated than such simple disk models. Basically all PMS objects are spectrally and photometrically variable, differing only in the amplitude and rate of variability. This variability includes also the NIR and mid-IR wavelengths where dust emission dominates (e.g., Chen & Jura 2003; Grinin 2000; Herbst & Shevchenko 1999; Skrutskie et al. 1996; Liu et al. 1996; Hutchinson et al. 1994; Prusti & Mitskevich 1994).

While some mid-IR variability can be attributed to variations in the stellar (or accretion) heating of the dust, many of these variabilities are *not* accompanied by changes in the luminosity of the central source. Such cases are a clear sign of dust dynamics producing modulations in the dust emission and/or stellar obscuration. On top of that, Vinković (2006) showed analytically that the dust sublimation zone of optically thick dusty disks cannot be constrained purely by radiative transfer. Sublimation leads to vertical optical thinning of the disk, which, combined with dust dynamics, leads to entirely new radiative transfer solutions. This result demonstrates that inferring a realistic geometry of dust distribution in the inner disk region of optically thick protoplanetary disks requires dust dynamics as well as radiative transfer.

Although the NIR visibilities are currently observed with a limited u-v coverage, dust dynamics responsible for strong variabilities should be detectable in multiepoch visibility observations. In addition, the newly employed NIR closure phase measurements enable interferometric detections of dusty disk inhomogeneities, as recently demonstrated in the case of AB Aur (Millan-Gabet et al. 2006b). Time evolution of such brightness asymmetries may significantly improve our understanding of processes responsible for the infrared variability of YSOs.

This is an important topic because current disk models have problems in explaining variabilities caused by transient dust obscurations of the central star (UXOR variables). This variability is manifested as changes in dust extinction, accompanied by the "blueing" effect and increased polarization at minima (Shakhovskoj et al. 2005; Rodgers et al. 2002; Rostopchina et al. 2001; Grinin et al. 1994, 2001; Grinin 2000; Skrutskie et al. 1996; Hutchinson et al. 1994). The photometric minima effects are a result of increased relative contribution of scattered starlight by dust in the total spectrum (Natta & Whitney 2000).

Temporal properties of obscuration events affecting visual and NIR wavelengths indicate that dust clouds usually appear in the inner disk regions at or close to the dust sublimation zone. If they belong to inhomogeneities *constrained to the disk*, then disk inclinations have to be large (Dullemond et al. 2003). The necessity for such a correlation was originally suggested by Natta et al. (1997). If we assume the most optimistic inner disk puffing of $H/R \sim 0.2$ (Vinković et al. 2006), then the line of sight would be affected by the inner disk when inclination angles are $i \gtrsim 80°$. This is inconsistent with the imaging data, which show disks with smaller inclination angles. In particular, the UXOR star CQ Tau (Shakhovskoj et al. 2005) has $i = 48^{+3}_{-4}$ deg derived from the NIR visibilities (Eisner et al. 2004), $i = 33° \pm 5°$ from the mid-IR imaging (Doucet et al. 2006), and $i \sim 60°-70°$ from millimeter imaging (Testi et al. 2003), while the UXOR star VV Ser has $i = 42^{+6}_{-2}$ deg derived from the NIR visibilities (Eisner et al. 2004).

We do not agree with the interpretation by Isella et al. (2006) that their derived disk inclinations (from fits to the NIR visibility) of $40°-55°$ for CQ Tau and $50°-70°$ for VV Ser are in agreement with the dust obscuration model. These inclinations would

actually support the idea of dust clouds being ejected to $\gtrsim 9$ (CQ Tau) and $\gtrsim 4.5$ (VV Ser) vertical scale heights above the dusty disk, which would dynamically decouple them from the disk (i.e., their dynamics would not be controlled by gas drag any more).

4.2. *Are Dusty Halos a Plausible Option?*

Dust obscuration events are easier to explain if we allow for a possibility of dust clouds being ejected to moderate polar angles above the disk midplane. Notice that this would still imply a dependence of variability on the inclination angle, which can explain the observed weak correlation between inclinations measured in $v \sin i$ and the amplitude of photometric variability (Grinin & Kozlova 2000). Similar correlation between the observed polarization and $v \sin i$ does not exist, but polarimetry supports the idea of a flattened halo above the disk (Yudin 2000). In addition, numerical models reproduce photometric and polarimetric variability of UXORs using the ad hoc assumption of obscuring dust clouds above the scattering dusty disk (Natta & Whitney 2000). We note that the variable accretion luminosity model put forward by Herbst & Shevchenko (1999) in order to explain the variability of UXOR objects was successfully challenged by the proponents of dust obscuration model (Rostopchina et al. 2001; Grinin et al. 2001; Grinin 2000).

Once a cloud is out of the dense gaseous disk, gas drag force becomes negligible and radiation pressure takes over. The cloud would be eventually blown away, creating a dusty halo-like outflow above the disk. Changes in such an outflow would manifest itself by changes in the NIR and mid-IR thermal emission. This IR variability is not dependent on the inclination angle, assuming optically thin emission. It would also be uncorrelated with the stellar spectrum variability. Although simultaneous visual and infrared observations are rare, such variability events have been documented (Chen & Jura 2003; Eiroa et al. 2002; Prusti & Mitskevich 1994; Hutchinson et al. 1994). Particularly interesting is the case of HD 163296, in which Sitko et al. (2004) detected an event of a major increase in the NIR and mid-IR emission. Since *Hubble Space Telescope* imaging shows a Herbig-Haro flow from this star (Grady et al. 2000b), they conclude that the observed infrared "flare" is possibly an ejection of a forthcoming Herbig-Haro object. If correct, this would directly link stellar outflow with the infrared variability due to dusty outflow.

Unfortunately, despite these seemingly convincing arguments, the existence of a dusty outflow is not straightforward and obvious. The biggest drawback in halo models is the lack of a known force capable of lifting a dust cloud out of the disk. The common assumption in circumstellar disk modeling is that gravity and gas drag do not allow dust to exit the high-density gaseous disk. Hence, the existing studies of NIR visibilities are dominated by disk models. Circularly symmetric images are sometimes invoked as a feature of dusty outflows not in agreement with NIR interferometry observations. However, in § 3.2 we argue that this is an ill-formed argument because halos can certainly display asymmetric images.

There was great excitement for some time about the possibility of cometary activity in Herbig Ae/Be stars detected in spectral line variations. This is called the β Pictoris phenomenon, after the same effect first observed in the dust debris disk of β Pic (Grady et al. 2000a). According to this interpretation, accretion episodes accompanied by redshifted absorption components in a number of metal lines are signatures of infalling evaporating comets. This would nicely fit into the above scheme of transient dust clouds. Unfortunately, further observations showed that the composition of infalling gas is consistent with the accretion disk gas (Natta et al. 2000), while numerical models revealed that

spectral signatures of comets cannot be detectable due to suppression by strong stellar winds in Herbig Ae/Be stars (Beust et al. 2001). Since then there have been no other suggestions for a process that could lift a dust cloud out of the disk.

A new imperative to explore dusty halos may come from the NIR visibility studies. The large NIR excess (often called the NIR "bump") of Herbig Ae/Be stars requires a vertical disk puffing at the inner disk edge (Isella et al. 2006; Dullemond et al. 2001). The NIR images based on this model have a large skewness: the brightness ratio between two opposite sides of the image centered on the star. Monnier et al. (2006) recently measured the NIR interferometry closure phases that can reveal the amount of skewness and found that observations do not support model predictions.[2] However, their claim is based mostly on high-L objects that do not exhibit visibilities consistent with the puffed-up disks anyway (see § 3.3.2). The main question is whether low-L Herbig Ae/Be stars can be described with this model or not. It turns out that closure phases are inconclusive for their skewness determination due to insufficient telescope resolution.

On the other hand, detailed modeling of the NIR visibilities with the puffed-up disk model is not successful in reproducing strong NIR bumps (MWC 758 and VV Ser; Isella et al. 2006). It was exactly these objects with a strong NIR bump that Vinković et al. (2006) point out as the most puzzling and most difficult to explain. The model also has problems with reconciling variability of UXOR stars with disk inclinations derived from the model, as already described above. Despite these difficulties, the model of curved puffed-up rims by Isella et al. (2006) is quite promising and represents the most advanced description of the inner disk region so far.

4.3. *Dust Grain Size in the Inner Disk Region*

Dust properties of the inner protoplanetary disk can also be deduced from the models of observed NIR visibilities. Since in § 3.3.2 we argue that NIR visibilities of high-L objects are not dust related, we limit our discussion on dust grain size to low-L YSOs only.

As already described in § 3.1, the inner radius of optically thick multigrain disks is controlled by the largest grains in the mix. Also, dust growth and dynamics may change the opacity structure of the inner disk and form a large optically thin zone populated by big ($\gtrsim 1\ \mu$m) grains extending closer to the star than the optically thick part of the disk. Results from § 3.1 support models of optically thick inner disks containing big grains. Smaller grains can hide inside the dusty disk, but we can see only big grains that populate the disk surface and shield smaller grains from the direct stellar heating. Dusty halo models of NIR visibilities also favor micron-size grains, but no larger than $\sim 10\ \mu$m (see § 3.2). Visibilities are, therefore, clearly suggesting that circumstellar dust exists in the region where submicron grains cannot survive when directly exposed to the stellar radiation.

Presence of big grains in the inner disk has been suggested before. Grady et al. (1995) modeled variations in the UV and visual spectra of UX Ori and obtained the best fit with grains $\geq 0.15\ \mu$m, which suggests considerable grain growth in comparison with the interstellar medium dust. Van Boekel et al. (2004) obtained spectra from the 1–2 AU zone of the immediate surrounding of several low-L Herbig Ae/Be stars using mid-IR interferometry. These spectra are dominated by micron-size thermally processed (crystalline) dust grains, which differs from the outer (2–20 AU) region where grains are smaller ($\sim 0.1\ \mu$m) and less crystalline. This is in agreement with results based on the NIR visibilities, where we expect such a grain size gradient due to dust sublimation. Small grains ($\lesssim 0.1\ \mu$m) around low-L Herbig Ae/Be stars sublimate at $\gtrsim 1$ AU, while micron-size grains can survive within 1 AU. These big grains populate the inner disk surface and dominate detected visibilities and spectra of the inner disk.

4.4. *The Difference between High- and Low-L YSOs*

The clear distinction between visibilities of low- and high-L YSOs may be a sign of more extensive dissimilarities between these two classes of objects. The change in circumstellar environment detected by visibilities appears at $\sim 10^3\ L_\odot$, which corresponds to the spectral type of about B3–B5 during the PMS phase. Here we point out some other significant changes in the YSO properties that happen around that spectral type.

Dispersal of circumstellar gas.—The mean gas density within a radius of 0.8 pc around high-L Herbig stars decreases by almost 2 orders of magnitude during their fast ($\lesssim 3 \times 10^5$ yr; Palla & Stahler 1993) evolution to the main sequence (Fuente et al. 1998). In contrast, environments of low-L stars experience a decrease of less than an order of magnitude. The NIR interferometry targets high-L objects that have still not dispersed their immediate environment. In § 3.3.2 we speculate that disk accretion rates under such conditions are high enough to enable a gaseous accretion disk to dominate the NIR emission and visibilities. This differs from low-L objects, where disks have time to evolve to the point where accretion rates become low enough to make the gaseous disk transparent, allowing dust emission to dominate the NIR.

Disk mass.—Disk masses in high-L Herbig stars are significantly lower than in low-L stars (Fuente et al. 2003). The trend is most noticeable in the ratio of disk to stellar mass, but it is also significant when the absolute disk mass is considered. It could be that these stars evolve through the PMS phase too quickly to accrete a massive disk before the star disperses its circumstellar environment.

Radiation pressure.—Detailed calculations of radiation pressure force on dust grains are very complicated and uncertain due to our limited knowledge of geometrical properties of individual dust grains (Burns et al. 1979). Nevertheless, we can exploit some general properties of the ratio of radiation pressure force to gravity, β, and derive an estimate for the size of grains repelled by the star ($\beta > 1$). The ratio β is generally proportional to $L_\star/M_\star$. Differences in the shape of stellar spectrum, grain refractive indices, and grain density can scatter the value of β by an additional order of magnitude (Burns et al. 1979). But luminosity differences between low- and high-L YSOs are so large that, in the first approximation, a comparison of β-values in YSOs is dominated by $L_\star/M_\star$. A PMS star of $L_\star = 10^3\ L_\odot$ has $M_\star \sim 6\ M_\odot$ (Palla & Stahler 1993), which means ~ 170 times larger β than in the solar system. High-L objects have even larger $L_\star/M_\star$ and hence even larger β. The Sun can eject dust particles of $\sim 0.2\ \mu$m in size (Landgraf et al. 1999; Burns et al. 1979), while other particles smaller than $\sim 10\ \mu$m in the solar system have $\beta \sim 0.01-1$. This means that we can safely assume that YSOs of $10^3\ L_\odot$ repel all dust grains smaller than $\sim 10\ \mu$m. In general, high-L YSOs have this limit at grain sizes larger than 10 μm because their luminosity is $> 10^3\ L_\odot$. It is difficult to maintain dusty structures around high-L objects with such high values of β. A dusty halo would be very efficiently dispersed. Puffed-up disk rims cannot maintain their vertical stability and would be efficiently blown away. Only dust within the optically thick gaseous disk or strongly dragged by gas toward the star can resist the radiation pressure force. The

---

[2] Monnier et al. (2006) suggest that the curved puffed-up rim model by Isella & Natta (2005) may be more suitable, but notice that this model also produces images with a large skewness (Isella et al. 2006).
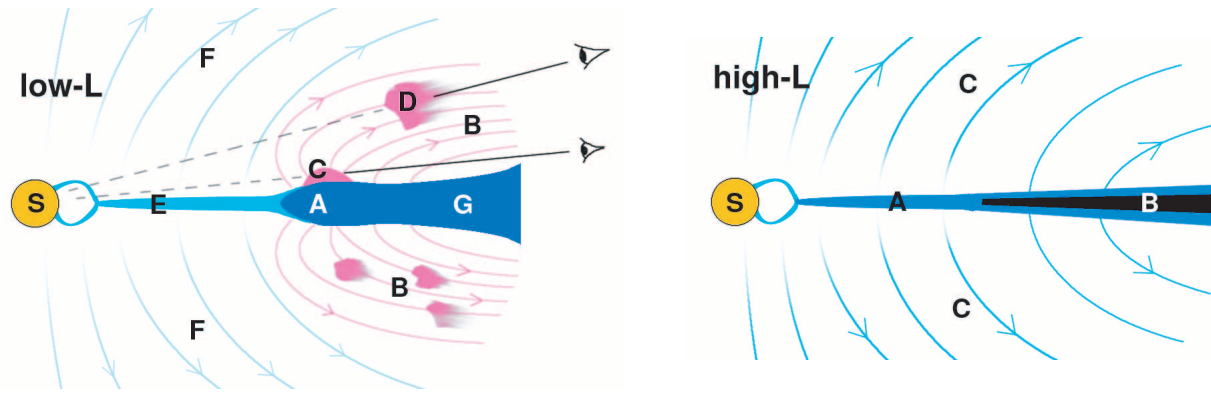
Fig. 12.—Emerging picture of the inner protoplanetary disk structure based on observed properties of high- and low-L YSOs. *Left*: Low-L objects have two competing models explaining their NIR visibilities and anomalously high NIR excess: (A) puffed-up inner disk rim and (B) dusty outflow creating a halo around the inner disk. Detected variability due to dust obscuration events suggests that either (C) the height of the puffed-up rim is variable and temporarily blocks the view toward the star or (D) clumps of dust appear in the dusty outflow and occasionally intercept the line of sight. The disk inside the zone of dust sublimation (E) is optically thin, while the rest is optically thick (G) due to dust. Gaseous stellar and disk winds (F) are also present. *Right*: High-L YSOs have a simpler structure. The star is surrounded by an optically thick gaseous accretion disk (A), which extends much closer to the star than the dust sublimation distance. But dust still may survive within the optically thick disk interior (B). Intense gaseous stellar and disk winds (C), combined with the stellar radiation pressure, are efficiently dispersing the surrounding environment. "S" marks the star.

situation is completely different for low-L objects. A 10^2 $L_\odot$ Herbig star has $L_\star/M_\star \sim 30$ (Palla & Stahler 1993); hence, the upper grain size limit of dust with $\beta \gtrsim 1$ is in the micron range. Curiously enough, this is consistent with smaller grains not surviving in the surface of the inner disk (see § 4.3).

Variability.—The range of photometric variabilities of high-L YSOs is much smaller ($\Delta V \lesssim 1.5$ mag) than that of low-L YSOs ($\Delta V \lesssim 6$ mag; Rodgers 2001; Herbst & Shevchenko 1999; Bibo & The 1991; Finkenzeller & Mundt 1984). This dependence of variability on luminosity is not understood. It may be that high luminosities are masking underlying accretion variabilities (unlike FU Ori stars where the stellar luminosity is much smaller than the accretion luminosity) or that dust sublimates so far away from the star that the probability for a transient dust obscuration is highly reduced (Grinin & Kozlova 2000). NIR visibilities, however, indicate that differences in the geometry of circumstellar matter distribution may be the reason. Another interesting property of the variability data is the correlation between the NIR flux excess and the range of variability amplitudes. Herbst & Shevchenko (1999) show this for Herbig Ae/Be stars by plotting the variability range in V band against the ratio of NIR excess luminosity to the stellar luminosity. Skrutskie et al. (1996) show this for T Tau stars by plotting variations of intrinsic $(K - L)$ color excess against the amplitude of the K-band variability. If the puffed-up inner dusty disk rim model is responsible for V-band variability (which we challenge; see § 4.1), then this correlation indicates temporal variations in the rim's height. The halo model, on the other hand, explains this correlation by connecting the amount of dust in the halo with the dynamics of dusty outflow. A larger NIR flux requires a larger optical depth of the halo, which in turn is a result of enhanced dust dynamics supplying the halo with dust. Side effects of this enhanced dynamics are dust obscuration events and NIR emission variabilities. Since the existence of such a halo is consistent only with low-L YSOs (see § 3.2), the variability amplitude is smaller in high-L YSOs because they lack the halo and its dust dynamics. Unfortunately, the current data are not sufficient for establishing which theory is correct.

5. SUMMARY

We have reviewed all published NIR (H and K band) visibility data of YSOs and devised a method for their model-independent

comparison. The method is based on scaling the distance of objects and their luminosity out of the measured baseline (eq. [1]). This removes the apparent dependence of the object's size on (1) its distance and (2) radiative transfer scaling due to luminosity. Hence, the visibility dependence on scaled baseline detects inherent differences in the geometry of circumstellar matter distribution without applying any additional theoretical model-dependent assumption.

The comparison shows a clear distinction between low-L YSOs ($L_\star \lesssim 10^3$ $L_\odot$) and high-L YSOs ($L_\star \gtrsim 10^3$ $L_\odot$), as already suggested by previous studies (Monnier et al. 2005; Eisner et al. 2004). Low-L visibilities cluster at spatial scales ~ 7 times larger than scales derived from the visibility clustering of high-L YSOs. Next, we analyze the observed visibility clusters with three types of image models. Modeling the whole data cluster instead of individual objects reveals or reaffirms some collective properties of these objects.

The first model is the uniform brightness ring, where we use dust sublimation as the boundary condition for the ring's inner radius. High-L YSOs are inconsistent with dust sublimation and appear much too small. The model was also not successful in explaining the size of the T Tau cluster. These stars appear slightly larger than model predictions. The model was more successful in low-L Herbig Ae/Be stars where the visibility cluster can be modeled with optically thick rings of $0°$–$60°$ inclination and a dust sublimation temperature of ~ 1500 K. The second model is the optically thin dusty halo. It explains the T Tau cluster with halos of ~ 0.2–1.0 visual optical depth. Low-L Herbig Ae/Be stars require optical depths of ~ 0.15–0.8. Halos made of micron-size grains provide the best fit to these data clusters. Finally, the third model is a classical accretion disk. We use this model on high-L Herbig Be stars and show that it can accommodate observed visibilities. The model does not constrain the accretion rate because equally successful fits can be built with $\dot{M}_{acc} = 0$ to 10^{-4} $M_\odot$ yr^{-1}. We argue, however, that the NIR emission from accretion disks must be due to gas and not dust; hence, accretion rates must be high in order to produce required thermal emission from the gas.

We also discuss variability properties of YSOs and made an attempt to incorporate them into the existing models of inner protoplanetary disks. We argue that dust obscuration events detected

through photometric and spectroscopic variability are caused by dust clumps too high above the dense inner protoplanetary disk to be considered dynamically part of the disk. Instead, we advocate a model where dust is ejected out of the disk and blown away by the radiation pressure. This would create a clumpy dusty halo-like outflow above the inner disk. Unfortunately, we are not aware of any physical process that could lift the dust out of the disk. Without this process the only alternative is to assume that the inner disk rim is puffed up and undergoes occasional height variations responsible for dust obscuration events. But this model is also problematic because it requires disk inclinations lager than actually observed in objects with dust obscuration events. All these facets of the evidently complicated circumstellar environment of YSOs are sketched in Figure 12. Grain size also plays a very important role in this environment. We argued for large ($\gtrsim 1$ μm) grains in the surface of the inner disk region of low-L YSOs based on theoretical and observational evidence.

In addition to the difference in their visibility clusters, high- and low-L YSOs differ in many other observational aspects.

High-L Herbig Be stars (1) are much more efficient in dispersal of their circumstellar gas and dust, (2) have smaller disk masses, (3) have strong radiation pressure capable of destroying circumstellar dust structures made of grains up to 10 μm or more in size, and (4) are far less photometrically variable. All these properties clearly indicate that the geometry of circumstellar gas and dust distribution around high-L YSOs is fundamentally different from those in their lower luminosity counterparts. Our current understanding of these environments is far from satisfactory and largely incomplete.

REFERENCES

Acke, B., & van den Ancker, M. E. 2004, A&A, 426, 151
Acke, B., van den Ancker, M. E., & Dullemond, C. P. 2005, A&A, 436, 209
Akeson, R. L., Ciardi, D. R., van Belle, G. T., & Creech-Eakman, M. J. 2002, ApJ, 566, 1124
Akeson, R. L., Ciardi, D. R., van Belle, G. T., Creech-Eakman, M. J., & Lada, E. A. 2000, ApJ, 543, 313
Akeson, R. L., et al. 2005a, ApJ, 622, 440
———. 2005b, ApJ, 635, 1173
Bell, K. R., & Lin, D. N. C. 1994, ApJ, 427, 987
Berrilli, F., Corciulo, G., Ingrosso, G., Lorenzetti, D., Nisini, B., & Strafella, F. 1992, ApJ, 398, 254
Beust, H., Karmann, C., & Lagrange, A.-M. 2001, A&A, 366, 945
Bibo, E. A., & The, P. S. 1991, A&AS, 89, 319
Burns, J. A., Lamy, P. L., & Soter, S. 1979, Icarus, 40, 1
Calvet, N., Hartmann, L., & Kenyon, S. J. 1993, ApJ, 402, 623
Calvet, N., Hartmann, L., & Strom, S. E. 2000, in Protostars and Planets IV, ed. V. Mannings, A. P. Boss, & S. S. Russell (Tucson: Univ. Arizona Press), 377
Calvet, N., Muzerolle, J., Briceño, C., Hernández, J., Hartmann, L., Saucedo, J. L., & Gordon, K. D. 2004, AJ, 128, 1294
Cesaroni, R., Galli, D., Lodato, G., Walmsley, C. M., & Zhang, Q. 2007, in Protostars and Planets V, ed. B. Reipurth, D. Jewitt, & K. Keil (Tucson: Univ. Arizona Press), 197
Chavarria-K., C., de Lara, E., Finkenzeller, U., Mendoza, E. E., & Ocegueda, J. 1988, A&A, 197, 151
Chen, C. H., & Jura, M. 2003, ApJ, 591, 267
Chini, R. 1981, A&A, 99, 346
Cieza, L. A., Kessler-Silacci, J. E., Jaffe, D. T., Harvey, P. M., & Evans, N. J., II 2005, ApJ, 635, 422
Claria, J. J. 1974, A&A, 37, 229
Clarke, C. J., & Pringle, J. E. 2006, MNRAS, 370, L10
Cohen, M., Bieging, J. H., Welch, W. J., & Dreher, J. W. 1985, ApJ, 292, 249
Colavita, M., et al. 2003, ApJ, 592, L83
Danchi, W. C., Tuthill, P. G., & Monnier, J. D. 2001, ApJ, 562, 440
de Lara, E., Chavarria-K., C., & Lopez-Molina, G. 1991, A&A, 243, 139
de Winter, D., & van den Ancker, M. E. 1997, A&AS, 121, 275
Dorschner, J., Begemann, B., Henning, T., Jaeger, C., & Mutschke, H. 1995, A&A, 300, 503
Doucet, C., Pantin, E., Lagage, P. O., & Dullemond, C. P. 2006, A&A, 460, 117
Drew, J. E., Busfield, G., Hoare, M. G., Murdoch, K. A., Nixon, C. A., & Oudmaijer, R. D. 1997, MNRAS, 286, 538
Dullemond, C. P., & Dominik, C. 2005, A&A, 434, 971
Dullemond, C. P., Dominik, C., & Natta, A. 2001, ApJ, 560, 957
Dullemond, C. P., van den Ancker, M. E., Acke, B., & van Boekel, R. 2003, ApJ, 594, L47
Eiroa, C., et al. 2002, A&A, 384, 1038
Eisner, J. A., Hillenbrand, L. A., White, R. J., Akeson, R. L., & Sargent, A. I. 2005, ApJ, 623, 952
Eisner, J. A., Lane, B. F., Akeson, R. L., Hillenbrand, L. A., & Sargent, A. I. 2003, ApJ, 588, 360
Eisner, J. A., Lane, B. F., Hillenbrand, L. A., Akeson, R. L., & Sargent, A. I. 2004, ApJ, 613, 1049

Finkenzeller, U., & Mundt, R. 1984, A&AS, 55, 109
Friedemann, C., Riemann, H. G., Gurtler, J., & Toth, V. 1993, A&A, 277, 184
Friedjung, M. 1985, A&A, 146, 366
Fuente, A., Martin-Pintado, J., Bachiller, R., Neri, R., & Palla, F. 1998, A&A, 334, 253
Fuente, A., Rodríguez-Franco, A., Testi, L., Natta, A., Bachiller, R., & Neri, R. 2003, ApJ, 598, L39
Garcia Lopez, R., Natta, A., Testi, L., & Habart, E. 2006, A&A, 459, 837
Grady, C. A., Perez, M. R., The, P. S., Grinin, V. P., de Winter, D., Johnson, S. B., & Talavera, A. 1995, A&A, 302, 472
Grady, C. A., Sitko, M. L., Russell, R. W., Lynch, D. K., Hanner, M. S., Perez, M. R., Bjorkman, K. S., & de Winter, D. 2000a, in Protostars and Planets IV, ed. V. Mannings, A. P. Boss, & S. S. Russell (Tucson: Univ. Arizona Press), 613
Grady, C. A., et al. 2000b, ApJ, 544, 895
Green, J. D., Hartmann, L., Calvet, N., Watson, D. M., Ibrahimov, M., Furlan, E., Sargent, B., & Forrest, W. J. 2006, ApJ, 648, 1099
Grinin, V. P. 2000, in ASP Conf. Ser. 219, Disks, Planetesimals, and Planets, ed. F. Garzón et al. (San Francisco: ASP), 216
Grinin, V. P., & Kozlova, O. V. 2000, Astrophysics, 43, 239
Grinin, V. P., Kozlova, O. V., Natta, A., Ilyin, I., Tuominen, I., Rostopchina, A. N., & Shakhovskoy, D. N. 2001, A&A, 379, 482
Grinin, V. P., The, P. S., de Winter, D., Giampapa, M., Rostopchina, A. N., Tambovtseva, L. V., & van den Ancker, M. E. 1994, A&A, 292, 165
Hartmann, L., & Kenyon, S. J. 1996, ARA&A, 34, 207
Hartmann, L., Kenyon, S. J., & Calvet, N. 1993, ApJ, 407, 219
Herbig, G. H., Andrews, S. M., & Dahm, S. E. 2004, AJ, 128, 1233
Herbst, W., & Shevchenko, V. S. 1999, AJ, 118, 1043
Herbst, W., Warner, J. W., Miller, D. P., & Herzog, A. 1982, AJ, 87, 98
Hernández, J., Calvet, N., Briceño, C., Hartmann, L., & Berlind, P. 2004, AJ, 127, 1682
Hillenbrand, L. A., Strom, S. E., Vrba, F. J., & Keene, J. 1992, ApJ, 397, 613
Hofmann, K.-H., Balega, Y., Ikhsanov, N. R., Miroshnichenko, A. S., & Weigelt, G. 2002, A&A, 395, 891
Hutchinson, M. G., Albinson, J. S., Barrett, P., Davies, J. K., Evans, A., Goldsmith, M. J., & Maddison, R. C. 1994, A&A, 285, 883
Isella, A., & Natta, A. 2005, A&A, 438, 899
Isella, A., Testi, L., & Natta, A. 2006, A&A, 451, 951
Ivezić, Ž., & Elitzur, M. 1996, MNRAS, 279, 1011
———. 1997, MNRAS, 287, 799
Ivezić, Ž., Nenkova, M., & Elitzur, M. 1999, User Manual for DUSTY, Univ. Kentucky Internal Rep.
Johns-Krull, C. M., & Valenti, J. A. 2001, ApJ, 561, 1060
Kenyon, S. J., Yi, I., & Hartmann, L. 1996, ApJ, 462, 439
Lada, C. J. 1985, ARA&A, 23, 267
Landgraf, M., Augustsson, K., Grün, E., & Gustafson, B. Å. S. 1999, Science, 286, 2319
Levreault, R. M. 1988, ApJ, 330, 897
Liu, M. C., et al. 1996, ApJ, 461, 334
Lorenzetti, D., Giannini, T., Nisini, B., Benedettini, M., Elia, D., Campeggio, L., & Strafella, F. 2002, A&A, 395, 637

Lynden-Bell, D., & Pringle, J. E. 1974, MNRAS, 168, 603
Malbet, F., et al. 1998, ApJ, 507, L149
———. 2005, A&A, 437, 627
———. 2007, A&A, in press
Mannings, V., & Sargent, A. I. 1997, ApJ, 490, 792
Manoj, P., Maheswar, G., & Bhatt, H. C. 2002, MNRAS, 334, 419
Meeus, G., Waters, L. B. F. M., Bouwman, J., van den Ancker, M. E., Waelkens, C., & Malfait, K. 2001, A&A, 365, 476
Millan-Gabet, R., Schloerb, F. P., & Traub, W. A. 2001, ApJ, 546, 358
Millan-Gabet, R., Schloerb, F. P., Traub, W. A., Malbet, F., Berger, J. P., & Bregman, J. D. 1999, ApJ, 513, L131
Millan-Gabet, R., et al. 2006a, ApJ, 641, 547
———. 2006b, ApJ, 645, L77
Miroshnichenko, A., & Corporon, P. 1999, A&A, 349, 126
Monnier, J. D. 2003, Rep. Prog. Phys., 66, 789
Monnier, J. D., & Millan-Gabet, R. 2002, ApJ, 579, 694
Monnier, J. D., et al. 2005, ApJ, 624, 832
———. 2006, ApJ, 647, 444
Mora, A., et al. 2004, A&A, 419, 225
Muzerolle, J., Calvet, N., Hartmann, L., & D'Alessio, P. 2003, ApJ, 597, L149
Muzerolle, J., D'Alessio, P., Calvet, N., & Hartmann, L. 2004, ApJ, 617, 406
Muzerolle, J., Luhman, K. L., Briceño, C., Hartmann, L., & Calvet, N. 2005, ApJ, 625, 906
Natta, A., Grinin, V. P., Mannings, V., & Ungerechts, H. 1997, ApJ, 491, 885
Natta, A., Grinin, V. P., & Tambovtseva, L. V. 2000, ApJ, 542, 421
Natta, A., Testi, L., & Randich, S. 2006, A&A, 452, 245
Natta, A., & Whitney, B. A. 2000, A&A, 364, 633
Palla, F., & Stahler, S. W. 1993, ApJ, 418, 414
———. 2000, in Star Formation from the Small to the Large Scale, ed. F. Favata, A. Kaas, & A. Wilson (ESA SP-445; Noordwijk: ESA), 179
Pérez, M. R., van den Ancker, M. E., de Winter, D., & Bopp, B. W. 2004, A&A, 416, 647
Pogodin, M. A., Malanushenko, V. P., Kozlova, O. V., Tarasova, T. N., & Franco, G. A. P. 2006, A&A, 452, 551
Porter, J. M., Drew, J. E., & Lumsden, S. L. 1998, A&A, 332, 999
Prusti, T., & Mitskevich, A. S. 1994, in ASP Conf. Ser. 62, The Nature and Evolutionary Status of Herbig Ae/Be Stars, ed. P. S. The, M. R. Perez, & E. P. J. Van den Heuvel (San Francisco: ASP), 257
Przygodda, F., van Boekel, R., Àbrahàm, P., Melnikov, S. Y., Waters, L. B. F. M., & Leinert, C. 2003, A&A, 412, L43
Quanz, S. P., Henning, T., Bouwman, J., Ratzka, T., & Leinert, C. 2006, ApJ, 648, 472
Rodgers, B., Wooden, D. H., Grinin, V., Shakhovsky, D., & Natta, A. 2002, ApJ, 564, 405
Rodgers, B. M. 2001, Ph.D. thesis, Univ. Washington
Rostopchina, A. N., Grinin, V. P., & Shakhovskoi, D. N. 2001, Astron. Rep., 45, 51

Sandell, G., & Weintraub, D. A. 2001, ApJS, 134, 115
Shakhovskoj, D. N., Grinin, V. P., & Rostopchina, A. N. 2005, Astrophysics, 48, 135
Shepherd, D. S., & Churchwell, E. 1996, ApJ, 472, 225
Shevchenko, V. S., Ibragimov, M. A., & Chenysheva, T. L. 1991, Soviet Astron., 35, 229
Sitko, M. L., Carpenter, W. J., Lynch, D. K., Russell, R. W., Grady, C. A., Brafford, S. M., & Wooden, D. H. 2004, BAAS, 36, 1363
Skrutskie, M. F., Meyer, M. R., Whalen, D., & Hamilton, C. 1996, AJ, 112, 2168
Straizys, V., Meistas, E., Vansevicius, V., & Goldberg, E. P. 1989, A&A, 222, 82
Strom, K. M., Strom, S. E., Breger, M., Brooke, A. L., Yost, J., Grasdalen, G., & Carrasco, L. 1972, ApJ, 173, L65
Strom, S. E., Grasdalen, G. L., & Strom, K. M. 1974, ApJ, 191, 111
Terranegra, L., Chavarria-K., C., Diaz, S., & Gonzalez-Patino, D. 1994, A&AS, 104, 557
Testi, L., Natta, A., Shepherd, D. S., & Wilner, D. J. 2003, A&A, 403, 323
Testi, L., Palla, F., & Natta, A. 1998, A&AS, 133, 81
Tuthill, P. G., Monnier, J. D., & Danchi, W. C. 2001, Nature, 409, 1012
Tuthill, P. G., Monnier, J. D., Danchi, W. C., Hale, D. D. S., & Townes, C. H. 2002, ApJ, 577, 826
van Boekel, R., Min, M., Waters, L. B. F. M., de Koter, A., Dominik, C., van den Ancker, M. E., & Bouwman, J. 2005, A&A, 437, 189
van Boekel, R., Waters, L. B. F. M., Dominik, C., Bouwman, J., de Koter, A., Dullemond, C. P., & Paresce, F. 2003, A&A, 400, L21
van Boekel, R., et al. 2004, Nature, 432, 479
van den Ancker, M. E., Blondel, P. F. C., Tjin A Djie, H. R. E., Grankin, K. N., Ezhkova, O. V., Shevchenko, V. S., Guenther, E., & Acke, B. 2004, MNRAS, 349, 1516
van den Ancker, M. E., de Winter, D., & Tjin A Djie, H. R. E. 1998, A&A, 330, 145
van den Ancker, M. E., Wesselius, P. R., & Tielens, A. G. G. M. 2000, A&A, 355, 194
Vinković, D. 2006, ApJ, 651, 906
Vinković, D., Ivezić, Ž., Jurkić, T., & Elitzur, M. 2006, ApJ, 636, 348
Vinković, D., Ivezić, Ž., Miroshnichenko, A. S., & Elitzur, M. 2003, MNRAS, 346, 1151
Warren, W. H., & Hesser, J. E. 1978, ApJS, 36, 497
Weigelt, G., Balega, Y. Y., Hofmann, K.-H., & Preibisch, T. 2002, A&A, 392, 937
White, R. J., & Ghez, A. M. 2001, ApJ, 556, 265
Wichmann, R., Bastian, U., Krautter, J., Jankovics, I., & Rucinski, S. M. 1998, MNRAS, 301, L39
Wilkin, F. P., & Akeson, R. L. 2003, Ap&SS, 286, 145
Yudin, R. V. 2000, A&AS, 144, 285